Classification of obstructive breathing using the RESpeck monitor

Goda Savickaite

4th Year Project Report
Computer Science and Mathematics
School of Informatics
University of Edinburgh

2019

Abstract

Opioid analgesics are commonly used for relieving pain after surgery. They have dangerous self-effects such as disturbing and depressing the breathing which unless attended to promptly could be fatal. Previous studies in detecting these breathing abnormalities using signals produced by different measurement devices have been undertaken but there is still a need for an unobtrusive method which can accurately find breathing obstructions in a timely manner.

A RESpeck device containing a tri-axis accelerometer is hoped to be a better alternative to the existing devices because of an easy and convenient way of using it. In this project, signals generated from this monitor are compared against a well-known breathing measurement device called nasal cannula and predictions between two classes, namely normal and obstructed, are made. Two methods have been implemented on breath-to-breath basis focusing on their shapes and ratios, respectively. The latter one was used for defining the performance on one of the most dangerous obstruction periods, called cyclic obstructions. The analysis is presented together with the best results of both models.

Acknowledgements

I wish to thank everyone who was a part of this project. I would like to give special thanks to my supervisor Prof. D. K. Arvind who constantly supported me and gave valuable insights and advice throughout my final year. He was a great mentor who pushed me to go forwards and achieve the best I can. Undoubtedly, I would like to thank Dr. Gordon Drummond for all the help with biological interpretations of my analysis and knowledge about breathing in general. With his support I got to learn how to work with a new software and identify obstructed and normal breathing all by myself. Moreover, I am grateful to another two people, namely Darius Fischer and Andrew Bates, who helped me a lot when facing some technical difficulties. Lastly, I appreciate all the support from my family and friends, including our small project group with whom I had to share this journey with.

Table of Contents

Chapter 1

Introduction

Opioid analgesia is widely used for relieving pain for post-operative patients. The side-effects include respiratory depression resulting in a lower rate and depth of breathing which could even be fatal when unattended [1]. Moreover, serious breathing disturbances are caused leading to chronic diseases such as sleep apnea [2]. The main reason behind this is the disruption of usual flow of oxygen and CO2. "Opioids are highly effective at killing pain, but they can also kill people by depressing their breathing and at the same time sedating them so that it can be impossible for them to wake up from oxygen deprivation" states Professor Richard Horner, Chair in Sleep and Respiratory Neurobiology, University of Toronto. Upper airway tumours caused by inconsiderate consumption of morphine lead to deaths of patients [3]. Similarly, mortality in children due to post-operative codeine leading to respiratory depression was present [4]. The decrease in the breathing rate and depth is a common consequence of opioid analgesia [5]. A study has been conducted [4] which proposes that using morphine led to less than 80% of oxygen desaturation while the use of regional anesthesia (numbing a particular region of the body) never decreased the oxygen saturation to less than 87% which proves the negative effect of opioids on the oxygen intake for post-operative patients. Another research carried out [6] concludes that one of the types of hospital deaths is related to upper airway reductions led by oxygen desaturation after the dosage of opioids. Note that this desaturation of oxygen is most evident during sleep [7] which is the main concern in this project. Various measures to detect abnormalities in breathing during sleep were used (look at Chapter 3) but there is still a need of an automatic and noninvasive method for observing those obstructions made by opioids in advance.

The seriousness of opioids effect on breathing can be affected by various biological factors such as age, gender, ethnicity, etc. For instance, the rates of clearance are much lower for older people than younger generations [8]. Also, the apnoeic threshold, which is a concentration of CO2 required to maintain the breathing stimulated, is being affected by morphine in men with no indication of changes in women [9]. On the contrary, the hypoxic (a breathing mixture of gas containing less that 21% of oxygen) sensitivity decreases in women but not in men [9]. Moreover, Chinese patients are being distinguished as having higher rates of clearance after consuming morphine or

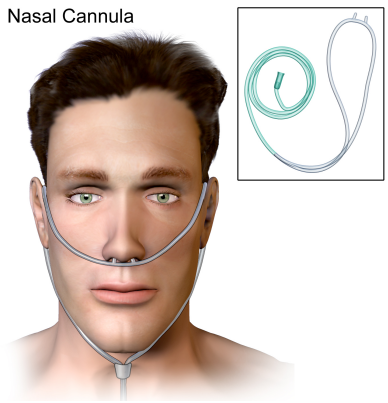

(a) Nasal cannula (licensed by BruceBlaus [CC BY-SA 4.0 (https://creativecommons.org/licenses/by-sa/4.0)])

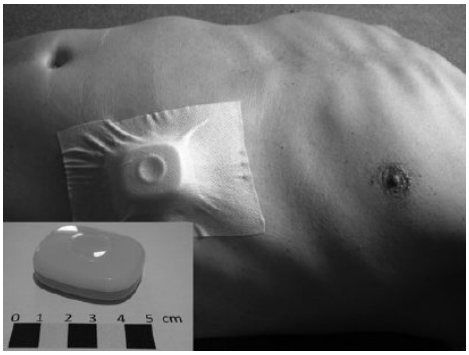

(b) RESpeck device [15]

Figure 1.1: Measurement tool used for the One-speck study

codeine while Caucasian population have a poor metabolism leading to a longer period of having high concentration of opioids [10].

The One-speck study conducted at the Royal Infirmary Edinburgh used the nasal cannula and the Respeck device for synchronously monitoring post-operative patients (more about this study in Section 2.2). Nasal cannulas, or nasal prongs, are widely used for monitoring the airflow going through the nose [11] which is an effective way of detecting some serious diseases caused by breathing abnormalities, such as upper airway resistance syndrome, sleep apnea and heavy snorer's disease [12] [13] [14]. However, wearing nasal cannula (look at Figure 1.1a) can sometimes be inconvenient since it often requires medical settings and an expert constantly monitoring the state of the breathing condition. That is why a new and easy to wear device called RESpeck with an installed accelerometer (look at Figure 1.1b) would be a much better solution in measuring the abnormalities caused by breathing because of the fact that it can be easily applied on the abdomen by only using a plaster. No clinical settings are required and measurements can even be done at home which would be accessible to a larger number of people.

In this project, breathing obstructions are divided into two categories based on the cannula signal. The idea behind this is that it is wanted to identify seriously obstructed periods (cyclic obstructions) more accurately because of their tendency to develop breathing related diseases.

1. **Cyclic obstructions**
   This breathing type is the most noticeable in the nasal cannula signal and can be considered as the most serious one because of its resemblance to the breathing of people with sleep apnea syndrome. Cyclic Obstructive Sleep Apnea is widely studied among researchers [16] which present the cyclic patterns in the heart rate and in the oro-nasal airflow signal derived from the nasal cannula. This kind of breathing can be seen in Figure 1.2a and be characterized by the following

pattern:

(a) Obstructed breathing (reduced airflow)

(b) Normal breathing (regular airflow)

In more detail, the magnitude of nasal pressure signal starts decreasing and the flattening of the waveform of inspiration appears which identifies the obstruction (Step (a)). Another indication for a breath being obstructed is the truncation appearing on the inspirations or a noticeable lack of flow comparing with the previous breaths. All these behaviours can be clearly seen in Figure 1.2a between cursors 1 and 2. After the obstruction period, a sequence of normal breaths with increased range of values of nasal pressure is evident which yields the compensation of effort and airflow put into previous breaths - a period of recovery (Step (b)). For a visualization look at Figure 1.2a between cursors 2 and 3. Note that the horizontal cursor divides the signal into two halves representing inspirations on the lower half and expirations on the upper one.

2. **Random obstructions**
   All the other breathing periods which are not classified to be cyclic are random. This means that the period contains a random distribution of two classes and most of the breaths in this type of breathing are ambiguous in a way that it is hard to tell whether a breath is obstructed or not while looking at the cannula signal. It can be seen in Figure 1.2b that some breaths are truncated in their shapes while others are smooth representing obstructed and normal breaths, respectively. Again, horizontal cursor divides the signal into inspirations and expirations.

The goal of this project is to identify airway obstructions in an unobtrusive way using a small but efficient and comfortable to wear device. Two different models, namely Shapelets (look at section 5.1) and Ratios method (look at Section 5.2) are implemented. Since Ratios method is context-sensitive (looks at previous breaths when making the prediction), the aim is to maximize the number of correctly classified breaths which are a part of cyclic obstruction pattern. All annotations of whether a breath is obstructed or not were made using only the cannula signal and are compared against the RESpeck signals, namely three accelerometer axes values and the breathing signal (more about them in Sections 2.2 and 2.3). Since the synchronous recordings of nasal prongs and RESpeck were made, these annotations are used to check the behaviour of the RESpeck signal when obstructions appear. Patterns are being inspected and detection of obstructions is made by building those two novel models.

The best performance found is using the Ratios method with a set of 15 features including all three accelerometer axes. The resulting accuracies for all and cyclic breaths are reported to be 75.12% and 92.77%, respectively, using 5-fold cross-validation. The best outcome of the Shapelets method was inspected to be 77.08% using accelerometer z axis.

The following is the outline of the report: Chapter 2 introduces the material needed for this project. It talks about the data collected and some insights which are essential for the next steps. Chapter 3 presents the current available methods for detecting obstructed breathing together with analysis made by other researchers. Moreover, solutions and models already existing are proposed and discussed for classification pur-

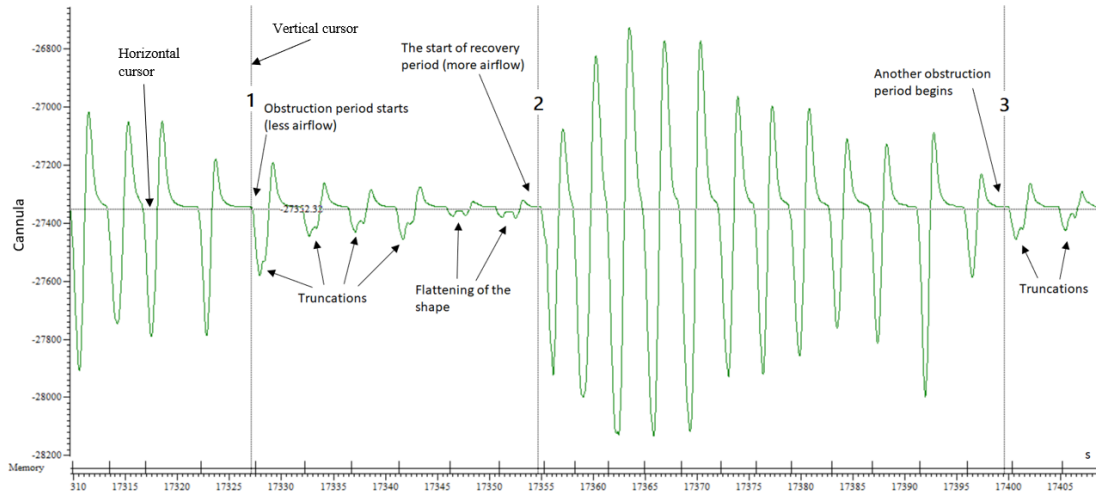

(a) Cyclic breathing obstructions

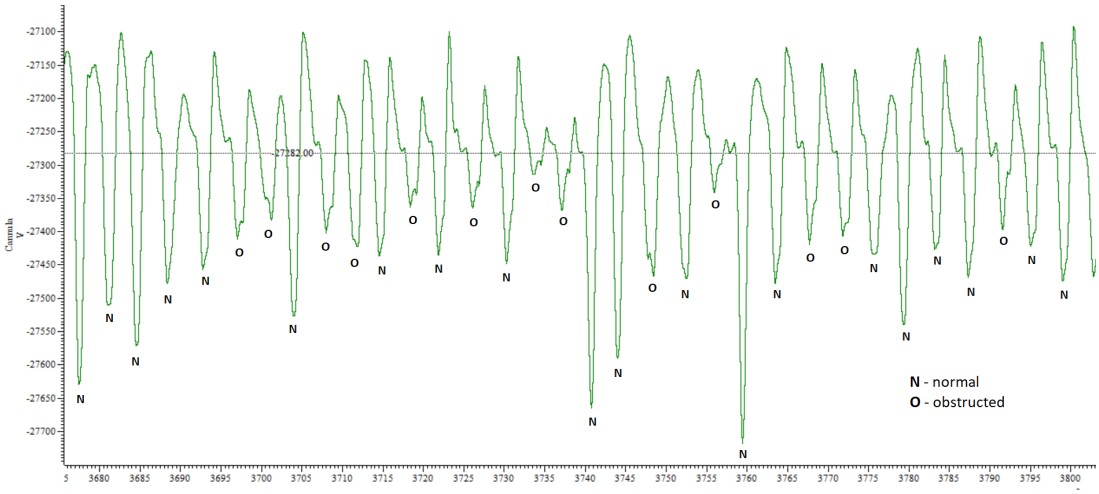

(b) Random obstructions

Figure 1.2: Types of breathing periods

poses. In the next chapter, namely Chapter 4, data preparation methods are presented together with some discussions regarding the shapes of breaths and feature engineering techniques used for finding the most representative patterns appearing in both classes. Chapter 5 describes the main methodology and best results achieved. Finally, conclusions are presented in Chapter 6 with some possible improvements and future work that could be done after this project.

Chapter 2

Background

This chapter will present tools used for data collection and introduce the background information related to the methods used for classification.

2.1 RESpeck device

Measuring the breathing of a person is a vital procedure in healthcare field. However, easily accessible and accurate measurements can be difficult. Most of the breathing controlling techniques require patients to breath directly through some apparatus which is often impractical and inconvenient (like nasal cannula [17]).

The RESpeck device, measuring 4.5 cm x 3.7 cm x 1.3 cm and weighing 17gms [18], is an unobtrusive wireless sensor containing three-axis accelerometer, designed for real-time respiratory monitoring with a minimal effort from the patient (can be seen in Figure 1.1b). This innovative sensor was made in The Centre for Speckled Computing at The University of Edinburgh and can be worn as a plaster on the chest with the data being transmitted wirelessly to a receiver.

2.2 One-speck study

The data used in this project came from the One-speck study and contains recordings from two patients who received post-operative morphine after their surgery. The duration and proportion of normal and obstructed breaths can be seen in Table 2.1. Note that in this Table only breaths which have more than 10 units for both inspirations and expirations are taken. In other words, it is being checked that breaths are not too short and last more than 20 timestamps, in total which is around $\frac{2}{3}$ of a second. Also, a check of whether a breath is not too long was done as well - only the ones that had length lower than 300 units which is around 9s were taken into account.

The selection of two patients was based on the appearance of cyclic breaths in their breathing periods (discussed in the Introduction) and the proportion of them is defined

Patient No.	No. of breaths	Duration	Proportion of normal breaths	Proportion of obstructed breaths	Proportion of cyclic breaths
1	1409	1h 34min	35.84%	64.16%	17.67%
16	1840	2h 11min	63.97%	36.03%	25.60%
In total:	3249	3h 45min	51.77%	48.23%	22.16%

Table 2.1: Statistical details of the two patients

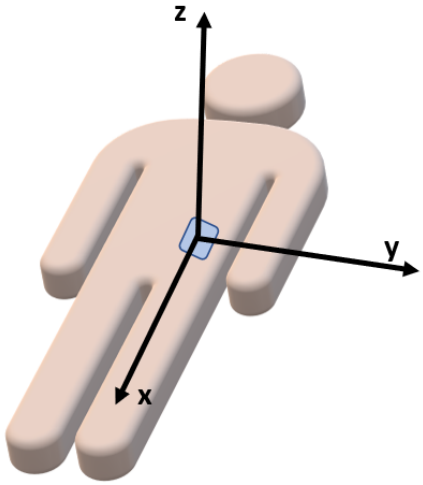

Figure 2.1: The orientation of RESpeck

in the same Table 2.1.

Note that both patients are quite different which is deliberate in order to find a generalized method. Patient 1 has more obstructed breaths than patient 16 whereas the latter has more cyclic episodes (described in the Introduction) than the former one. In total, there is 3h 45min worth of data used in this project.

One RESpeck placed on the abdomen was used to generate values of three axes of accelerometer which were also taken for the derivation of the breathing signal (more details in Section 2.3). The orientation of RESpeck for this study is visualized in Figure 2.1 with the corresponding x, y, z axes labeled.

Concurrently with the RESpeck sensor, another device, namely the nasal cannula, was used. Nasal cannula is a lightweight tube placed in the nostrils and used for airflow measuring. It measures the speed of air that passes through the nose with a maximum volume appearing when the signal hits 0. These nasal pressure values were imported to Spike which is a software for multi-channel analysis of the data [19]. It was used for the annotations made with the guidance of an experienced observer and exported to .csv files at the frequency of 32Hz. The marks for the start and end of inspirations were identified and the classification between two classes: normal and obstructed was made using four different memory channels. An example of cannula signal can be seen in Figure 1.2 where two different types of breathing are presented and explained in the Introduction. Note that the horizontal cursor placed at around -27300 divides

the plane into inspirations and expirations corresponding to lower and upper halves, respectively. During the inspiration the flow is going in the nose what can be seen by the curve going down the horizontal cursor and back. When it hits the cursor the flow is equal to 0. Similarly, when the signal is increasing starting from the horizontal cursor and the going back - patient exhales, flow is going out.

2.3 Breathing signal

As mentioned in the previous section, the data consists of three accelerometer values which were used for getting the breathing signal using the method described in the work of D. K. Arvind et al. [20]. The following parameters were used to get a smoothed breathing signal while applying the band-pass Butterworth filter:

- Activity cutoff = 100Hz. It is a movement threshold. If it is being exceeded (too much movement), the breathing algorithm is stopped.
- Min threshold = 0.001. The minimum threshold for an amplitude
- Max threshold = 0.14. The maximum threshold for an amplitude.
- Threshold filter size = 128. The number of samples used for calculating the RMS-threshold (Root Mean Squared threshold) for peak detection. Must be around two breaths long.
- Threshold factor = 4.2. Factor that the RMS-threshold from above is being multiplied.
- Pre-filter = 50. Smoothing before the calculation of the breathing signal.
- Post-filter = 50. Smoothing after the calculation of the breathing signal.
- Sampling frequency = 32Hz.

Using the Butterworth filter provides with the flattest frequency response it is possible in the pass band [21]. This leads to the resulting breathing signal having the same baseline throughout the whole recording.

Chapter 3

Related work

An overview of previous work done in investigating the obstructive breathing periods using signals extracted from various sleep studies.

Over the last decade a lot of research was conducted for detecting Sleep Apnea's (SA) episodes. Various processing and feature extraction techniques were used on signals like nasal air flow (we use this as the measurement for detecting obstructions in this report), oxygen saturation, electrical activity of the heart and brain (ECG and EEG, respectively) or even the breathing sound to identify SA. Even though the aim of this project is to detect obstructions which are not necessarily caused by SA but they might be an early identification of this disease. That is why previous work done in detecting Sleep Apnea is important and should be established here.

One of the methods for detecting obstructed breathing is called polysomnography (PSG) which is a sleep study and being conducted in a clinical environment with a necessity of having an experienced observer taking observations throughout the whole recording period. This is considered to be an inefficient, limited and quite expensive method for detecting obstructed sleeping episodes. During this study the measurements of the breath airflow, respiratory movement, oxygen saturation, body position, EEG, ECG, etc. [22] can be tracked. By measuring sleep variables of the signals got from PSG study, the diagnosis regarding the SA can be done [23]. Undoubtedly, this technique is very time-consuming and impractical, so the ability to substitute this with the RESpeck device would be a much cheaper and easier to use alternative.

The difficulties and impracticalities of PSG led T.Kim, J.W. Kim and K.Lee [24] to performing a classification method based on the breathing sound which was recorded as a part of PSG using an embedded microphone. An accoustic biomarker which consists of audio features extracted from the 5s long interval recordings of patient's breathing sound was used in this method. Another feature incorporated into this study was quantized transition matrix (qTM) which shows the distribution of transition patterns between low-level signal, and high-level signal magnitudes. Neural Networks, SVMs and simple logistics were evaluated for classification of four different classes of breathing episodes: normal, mild, moderate, severe using the acoustic biomarker and qTM as features. The best classifier found was simple binary model using thresholds

for different classes yielding the accuracy of 92.5%. The authors have demonstrated that it is possible to accurately predict breathing obstructions using just a breathing sound with no need of an experienced observer attending a full night PSG.

Pulse oximetry is a test which measures the level of oxygen saturation in the blood easily and noninvasively detecting even the smallest changes of oxygen flow through the whole body [25]. A small clip-like device is attached to a human's body and SpO_2 signal is being measured. By taking two common oxymetric indices and one non-linear metric of this pulse oximetry produced signal [26] implemented a three-layer Neural Network. This method achieved a great success reaching 93.3% accuracy.

The previous work of L.Almazaydeh, M.Faezipour and K.Elleithy was further improved using linear kernel Support Vector Machines (SVMs) [27]. This time they used 10 features extracted from 15s long intervals of Respiratory Rate of the ECG signal. The performance of the new method improved a lot constituting to 96.5%.

In 2013, Virtua Health System (VHS) prioritized the improvements in detecting the effects made by narcotic consumption by introducing a non-invasive capnography (measuring the level of carbon dioxide in a breath) and continuous pulse oximetry monitoring [28] in order to provide hospitals with a more practical use for monitoring respiratory data. For this new method only a nasal cannula worn over nose was needed in contrast with a regular monitoring which required a person being intubated. Even though this has ease up the measuring process it was still necessary to have physicians constantly tracking the process and making assumptions about the data they are getting which means the automatic detection of obstructions would be a much better solution to this new method introduced.

Another approach which was used to find obstructions in breathing using nasal cannula values was made by T. Aittokallio et al. [14]. Analysis on different inspiratory shapes was done and seven different categories were inspected and are presented in Figure 3.1. Note that the curves increase when there is more flow going through the nose while in this report negative values correspond to more pressure passing through. Hence, the shapes that are found in Figure 3.1 are mirror curves to the ones discussed in this project (an example can be seen in Figure 1.2). As it was discussed in the Introduction since no flattening of the waveform appears in class 1, it corresponds to a normal breath whereas other six classes are different categories of partial upper-airway inspiratory obstructions. Two years after conducting this analysis T. Aittokallio et al. found a way to detect seven classes of shapes using finite state machines [29] which were constructed in such a way that they would count the number and order of peaks in the shapes and based on that the prediction to one of seven categories was made. The result of this method was 94% of correctly classified waves.

It is being hoped that accelerometer values and the breathing signal show some differences in shapes as well when obstructions appear and analysis on that is done in Section 4.1 with the implementation of a new method in Section 5.1. This new model called Shapelets method was used by L. Ye and E. J. Keogh [30] in classifying different leaves species as it will be explained in Section 5.1. Another classification task where this method was implemented involves a real-time activity recognition [31]. Six different human activities including walking, going up/down the stairs and jogging

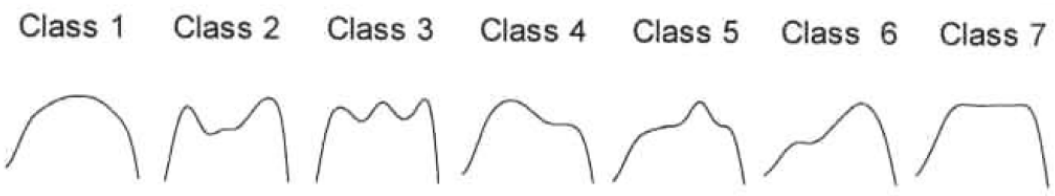

Figure 3.1: Shapes of inspirations in nasal cannula [29]

at different speed were performed and the accelerometer signal with respect to those was measured. Using Dynamic Time Warping a shapelet, or the best representative subsequence, was found with respect to each activity. The average accuracy of these activities was found to be 86% which is comparable to offline human activity recognition techniques where a transmission of data into the server is required leading to cost inefficiency.

Lastly, one attempt in classifying obstructed and normal breaths using RESpeck was already done by J. Murphy [32]. Only the breathing signal described in Section 2.3 was taken into analysis and different time and frequency features were engineered for machine learning models building. It was found that the decision tree of depth 6 and SVM with RBF Kernel (C=10,000, gamma=0.006) were the best classifiers resulting in 73.3% and 76.0% test accuracies, respectively. The baseline model, classifying all breaths as the dominant class was selected and showed an accuracy of 57.7% which yields that this result was improved by 18.3% with the best SVM classifier. Note, however, that this method does not take into account the continuity and context of breaths which is an important property in classifying breaths as it will be discussed in Section 5.2. Lastly, note that the breathing signal itself might not be enough to identify two classes of breaths because of different types of obstructions yielding contradictory patterns as described in Section 4.2. That is why the accelerometer values were taken into consideration when looking for the differences between obstructed and normal breaths in this project.

Chapter 4

Data analysis

The description of how the data was cleaned and prepared for the feature engineering and methods used for detecting those features.

4.1 Shapes

One of the first approaches considered for spotting the differences in patterns between normal and obstructed breaths is the shapes disregarding any scaling factors.

All three axes of accelerometer and the breathing signal were scaled to the same interval with an additional rolling mean of 5 for reducing noise and presenting clear shape patterns. Only the inspirations were taken into analysis because that is where most of the obstructions are present. This reasoning was confirmed by a private communication with Dr. Gordon Drummond. Two classes were separated as in Figure 4.1 which clearly suggests that both obstructed and normal breaths give relatively similar shapes. This was confirmed by finding a ”representative shape” which can be defined by first resampling all breaths to the median length of each class and taking the average of the signals of a particular class. For example, if the median length of an obstructed breath is med_len, then each obstructed breath of three accelerometer values and the breathing signal will be resampled to med_len. Then for finding the ”representative shape” of the breathing signal, all obstructed breaths are taken and the average of those resampled signals is found. The resulting ”representative shapes” can be seen in Figure 4.2. It can be observed that for both patients the trends in shapes are quite similar:

- Accelerometer x axis ($accel\_x$): For both patients the obstructed shape seems to be lower at the end of the inspiration. Overall, it does not seem to represent the classes very well.
- Accelerometer y axis ($accel\_y$): It is clear that the normal shape shows a more steady increase than the obstructed one.
- Accelerometer z axis: ($accel\_z$) The ”cup” of the normal shape appears faster than the one of an obstructed breath.

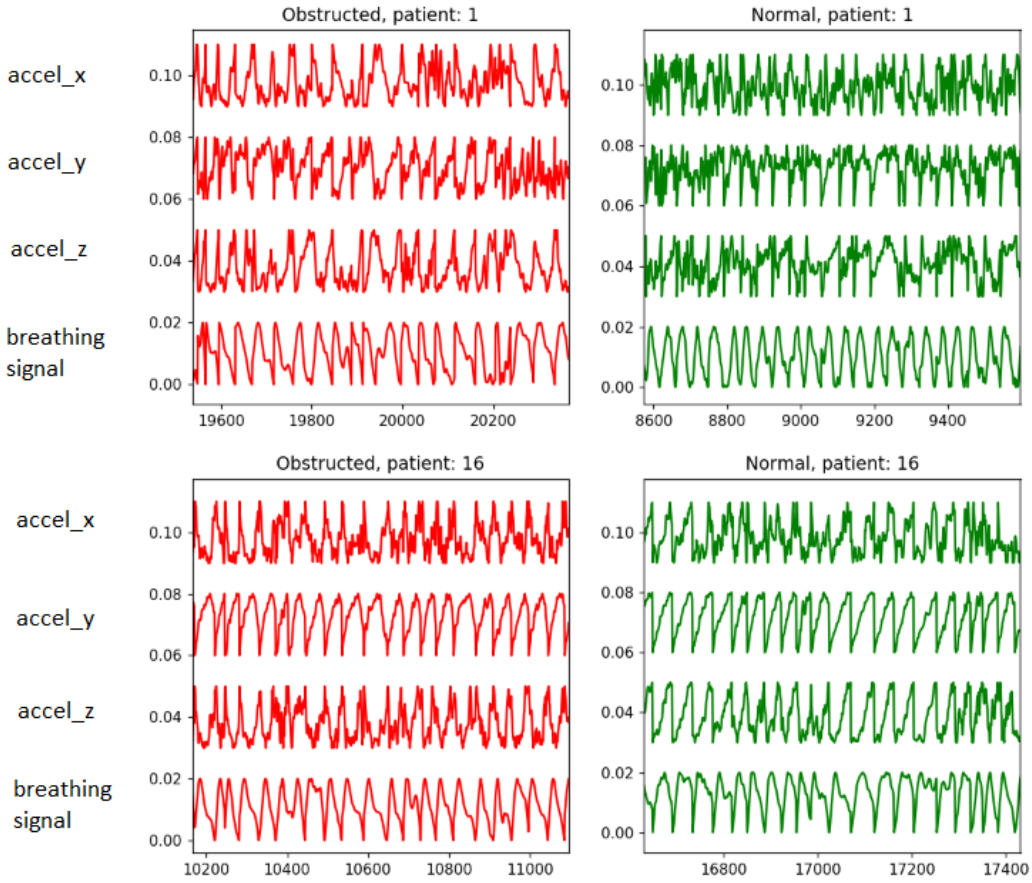

Figure 4.1: Separated normal and obstructed breaths shapes

- Breathing signal: The shape of normal breath appears to be wider and lower than the obstructed one.

Another interesting observation must be noted. The shapes of accelerometer values really depend on the body shape of the actual patient. As an example axis z can be taken since it represents the breathing changes the most since it corresponds to up-and-down movement of abdomen (look at Figure 2.1). Consider three different shapes of a person as in Figure 4.3 where solid line corresponds to the start of inspiration while the dashed one represents the end of it. The middle shape shows the case when the shape pattern (moving up and down) would be the most noticeable since the values are changing significantly when the abdomen goes up and down. In the meantime, first and third shapes of patients would lead to a smaller range of shapes noticeable. By looking at accelerometer z axis for both patients in Figure 4.4 (plotted using Spike) one can notice that different patterns are apparent when the switch between obstructed and normal breathing happens. For patient 1 in Figure 4.4a during the obstruction period there is a much more noticeable shape pattern than during the normal breathing. However, the opposite behaviour can be seen for patient 16: the shape pattern is more evident during the normal period. Even there is little research done on relating these axes to the shape of a person, it can still be stated that it highly influences the patterns appearing. Also, note that sometimes inspiration and expiration correspond to an increase or decrease

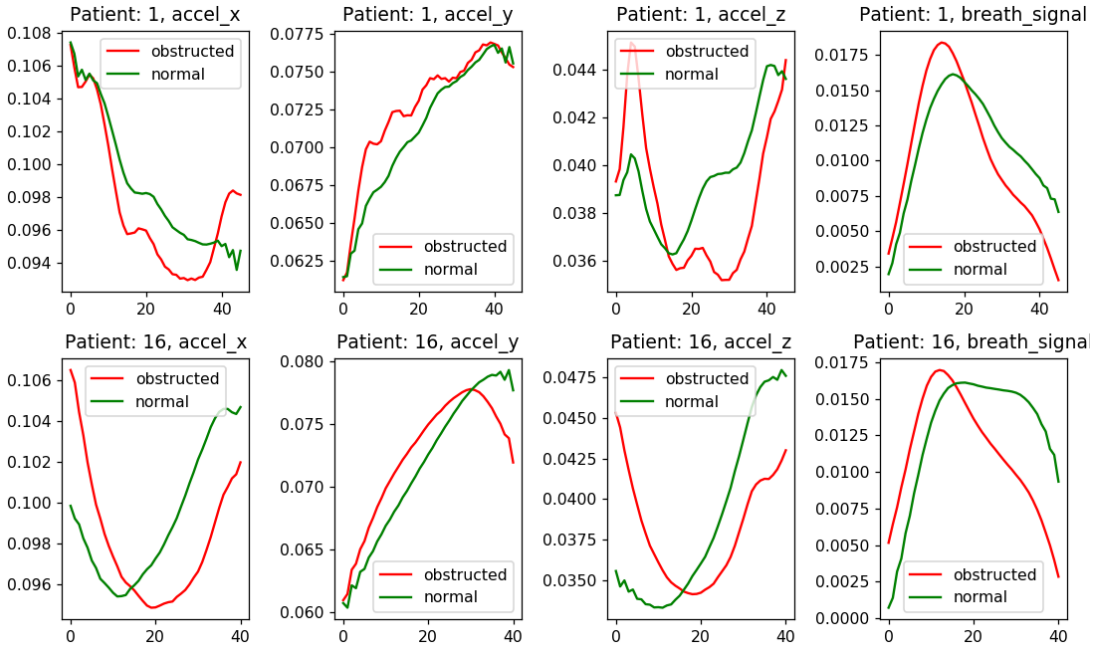

Figure 4.2: Representative shapes with respect to each accelerometer axis and the breathing signal

of a particular axis based on the shape of a person as well. Suppose the first shape in Figure 4.3 corresponds to an increase in x axis when inspiration happens, then the opposite behaviour would be apparent if the shape of the person would be similar to the third image in Figure 4.3. Note that in addition to this a slight movement of person's position can cause an effect of a "different body shape" which would lead to changes in these shape patterns which would be a limitation of the Shapelets method.

This analysis shows that even if shapes seem to be quite similar between classes with possible changes because of the body shape and movements, an attempt to automatically find the differences concerning shapes will still be made and is described in Section 5.1.

4.2 Scaling

As it was discussed in the previous section, the waveforms of both obstructed and normal breaths are quite similar visually when disregarding the scaling factors. That is why statistical tools measuring the changes in values must be incorporated. In this section, the focus is on the parallel comparison of nasal cannula and three accelerometer values with the breathing signal.

First of all, the differences between all five signals can be seen in Figure 4.4. These are the obvious examples of two cyclic breathing obstruction periods described in the Introduction with clear obstruction and recovery periods. For Patient 1 (Figure 4.4a) the obstructions appear before cursor one with a noticeable recovery period after it.

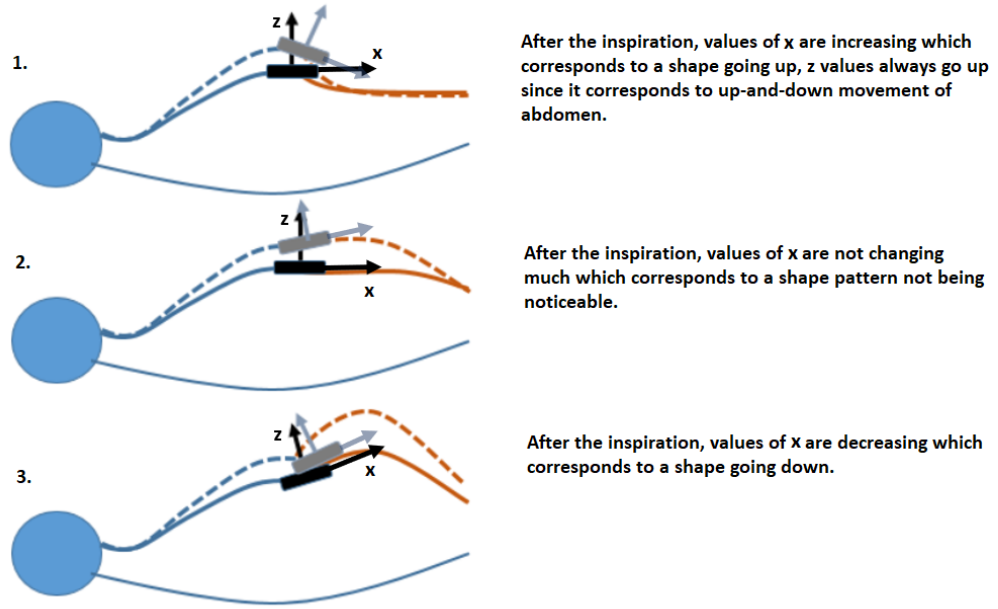

Figure 4.3: Body shapes

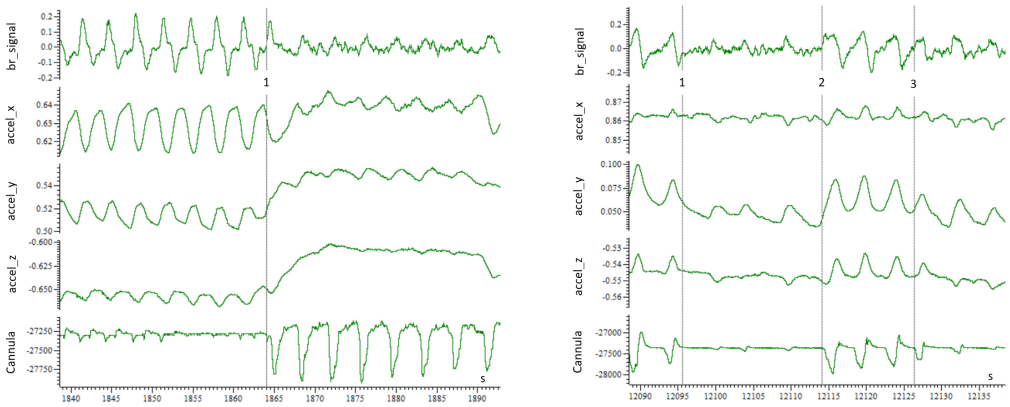

(a) Patient 1 (b) Patient 16

Figure 4.4: Combined cannula, accelerometer and breathing signal values during cyclic breathing obstruction period

Meanwhile, in Figure 4.4b, obstructed period of breathing can be seen between cursors 1 and 2 with a period of recovery starting at cursor 2 and ending at 3. Note that the values of accelerometer values are in terms of “g” - the acceleration due to gravity.

It is obvious from Figure 4.4 that cyclic patterns can be recognized when analyzing the accelerometer values. However, the changes in the axes are different from what it was observed for the cannula:

1. Axis x shows some differences in range or standard deviation while the changes in the scaling are different for each patient. Note that patient 1 presents an obvious increase of values meanwhile, that is not the case for patient 16.
2. Axis y presents obvious changes when the switch between two classes appears.

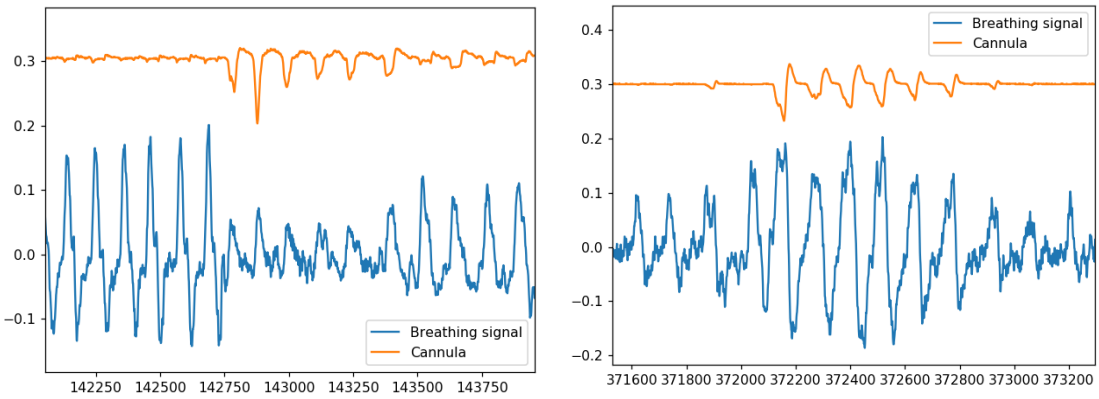

(a) Usual behaviour

(b) Contradictory behaviour

Figure 4.5: Combined cannula and breathing signal during cyclic breathing obstruction period

The values go much higher for the normal breathing period than the obstructed one.

3. Axis z presents similar patterns as axis y in Figure 4.4.

At the same time, the breathing signal, derived from three axes of accelerometer, is showing unstable behaviour. Most of the time, it presents a contrary behaviour to the nasal cannula (look at Figure 4.5a). During the obstruction period the magnitude of the breathing signal is increasing with no identification of flattening effect on the signal as it can be seen in the cannula signal. As before, the breathing signal behaves oppositely when the period of recovery occurs - the magnitude decreases. Note that in Figure 4.5 the values of cannula signal are scaled to match the breathing signal for visualization.

However, in some cases the behaviour of the breathing signal is the complete opposite to the one described above. Note that it is derived from the accelerometer values as described in Section 2.3. Hence, the notion of different body shapes can be the reason of inconsistent breathing signal. In Figure 4.5b it can be seen that obstructed breaths present values that are much lower than the ones for normal breaths contradicting the behaviour in Figure 4.5a. Note that both of these different behaviours can be seen in Figure 4.4 as well by looking at signal named *br_signal* which also presents two contrary behaviours of the breathing signal for both patients during cyclic breathing obstruction period. One of the reasons behind this is the possibility of a person breathing through his mouth during that period. In this way, movements on abdomen are still present but no airflow is going through the nose. Another possible explanation for this would be different types of obstructions involving more movement on the abdomen than most of the irregular breaths.

It was analyzed that contrary behaviour of the breathing signal is the property of patient 16 which leads to breathing signal features being not representative for the analysis.

4.3 Data Cleaning and Preprocessing

Before building the models the data was carefully selected by looking at the signals visually. All periods that seemed to have a lack of generalization throughout whole recordings were removed leaving only the data which is representative for generating features and building models.

4.4 Feature Engineering

Features were engineered by carefully analyzing the breathing signal and accelerometer axes while looking for statistical measures to find the most significant differences between normal and obstructed breaths. Since the marks given included the start and end of inspirations, statistical features were engineered for both inspirations, expirations and full breaths (except the length ratio explained below). The following statistics were analyzed:

- **Mean of the breathing signal, three accelerometer axes** ($mean$, $mean\_ins$, $mean\_exp$, $mean\_accel\_x$, $mean\_accel\_x\_ins$, $mean\_accel\_x\_exp$, $mean\_accel\_y$, $mean\_accel\_y\_ins$, $mean\_accel\_y\_exp$, $mean\_accel\_z$, $mean\_accel\_z\_ins$, $mean\_accel\_z\_exp$)
- **Standard deviation of the breathing signal, three accelerometer axes** (std, std_ins, std_exp, std_accel_x, $std\_accel\_x\_ins$, $std\_accel\_x\_exp$, std_accel_y, $std\_accel\_y\_ins$, $std\_accel\_y\_exp$, std_accel_z, $std\_accel\_z\_ins$, $std\_accel_z\_exp$)
- **Median of the breathing signal, three accelerometer axes** ($median$, $median\_ins$, $median\_exp$, $median\_accel\_x$, $median\_accel\_x\_ins$, $median\_accel\_x\_exp$, $median\_accel\_y$, $median\_accel\_y\_ins$, $median\_accel\_y\_exp$, $median\_accel\_z$, $median\_accel\_z\_ins$, $median\_accel\_z\_exp$)
- **The difference between the maximum and the mean of the breathing signal** ($max - mean$, $max - mean\_ins$, $max - mean\_exp$, $max - mean\_accel\_x$, $max - mean\_accel\_x\_ins$, $max - mean\_accel\_x\_exp$, $max - mean\_accel\_y$, $max - mean\_accel\_y\_ins$, $max - mean\_accel\_y\_exp$, $max - mean\_accel\_z$, $max - mean\_accel\_z\_ins$, $max - mean\_accel\_z\_exp$)
- **The difference between the minimum and the mean of the breathing signal, three accelerometer axes** ($min - mean$, $min - mean\_ins$, $min - mean\_exp$, $min - mean\_accel\_x$, $min - mean\_accel\_x\_ins$, $min - mean\_accel\_x\_exp$, $min - mean\_accel\_y$, $min - mean\_accel\_y\_ins$, $min - mean\_accel\_y\_exp$, $min - mean\_accel\_z$, $min - mean\_accel\_z\_ins$, $min - mean\_accel\_z\_exp$)
- **Maximum of the breathing signal, three accelerometer axes** (max, max_ins, max_exp, max_accel_x, $max\_accel\_x\_ins$, $max\_accel\_x\_exp$, max_accel_y, $max\_accel\_y\_ins$, $max\_accel\_y\_exp$, max_accel_z, $max\_accel\_z\_ins$, $max\_accel\_z\_exp$)
- **Minimum of the breathing signal, three accelerometer axes** (min, min_ins, min_exp, min_accel_x, $min\_accel\_x\_ins$, $min\_accel\_x\_exp$, min_accel_y, $min\_accel\_y\_ins$, $min\_accel\_y\_exp$, min_accel_z, $min\_accel\_z\_ins$,

min_accel_z_exp)

- **Range of the breathing signal, three accelerometer axes** (*range*, *range_ins*, *range_exp*, *range_accel_x*, *range_accel_x_ins*, *range_accel_x_exp*, *range_accel_y*, *range_accel_y_ins*, *range_accel_y_exp*, *range_accel_z*, *range_accel_z_ins*, *range_accel_z_exp*)
- **Skewness of the breathing signal, three accelerometer axes** (*skew*, *skew_ins*, *skew_exp*, *skew_accel_x*, *skew_accel_x_ins*, *skew_accel_x_exp*, *skew_accel_y*, *skew_accel_y_ins*, *skew_accel_y_exp*, *skew_accel_z*, *skew_accel_z_ins*, *skew_accel_z_exp*)
- **Kurtosis of the breathing signal, three accelerometer axes** (*kurtosis*, *kurtosis_ins*, *kurtosis_exp*, *kurtosis_accel_x*, *kurtosis_accel_x_ins*, *kurtosis_accel_x_exp*, *kurtosis_accel_y*, *kurtosis_accel_y_ins*, *kurtosis_accel_y_exp*, *kurtosis_accel_z*, *kurtosis_accel_z_ins*, *kurtosis_accel_z_exp*)
- **Quantiles of 0.1, 0.25, 0.75, 0.9 of the breathing signal, three accelerometer axes** (0.1*quant*, 0.1*quant_ins*, 0.1*quant_exp*, 0.25*quant*, 0.25*quant_ins*, 0.25*quant_exp*, 0.75*quant*, 0.75*quant_ins*, 0.75*quant_exp*, 0.9*quant*, 0.9*quant_ins*, 0.9*quant_exp*, 0.1*quant_accel_x*, 0.1*quant_accel_x_ins*, 0.1*quant_accel_x_exp*, 0.25*quant_accel_x*, 0.25*quant_accel_x_ins*, 0.25*quant_accel_x_exp*, 0.75*quant_accel_x*, 0.75*quant_accel_x_ins*, 0.75*quant_accel_x_exp*, 0.9*quant_accel_x*, 0.9*quant_accel_x_ins*, 0.9*quant_accel_x_exp*, 0.1*quant_accel_y*, 0.1*quant_accel_y_ins*, 0.1*quant_accel_y_exp*, 0.25*quant_accel_y*, 0.25*quant_accel_y_ins*, 0.25*quant_accel_y_exp*, 0.75*quant_accel_y*, 0.75*quant_accel_y_ins*, 0.75*quant_accel_y_exp*, 0.9*quant_accel_y*, 0.9*quant_accel_y_ins*, 0.9*quant_accel_y_exp*, 0.1*quant_accel_z*, 0.1*quant_accel_z_ins*, 0.1*quant_accel_z_exp*, 0.25*quant_accel_z*, 0.25*quant_accel_z_ins*, 0.25*quant_accel_z_exp*, 0.75*quant_accel_z*, 0.75*quant_accel_z_ins*, 0.75*quant_accel_z_exp*, 0.9*quant_accel_z*, 0.9*quant_accel_z_ins*, 0.9*quant_accel_z_exp*)
- **Number of times the mean of the breathing signal, three accelerometer axes is crossed** (*mean_cross*, *mean_cross_ins*, *mean_cross_exp*, *mean_cross_accel_x*, *mean_cross_accel_x_ins*, *mean_cross_accel_x_exp*, *mean_cross_accel_y*, *mean_cross_accel_y_ins*, *mean_cross_accel_y_exp*, *mean_cross_accel_z*, *mean_cross_accel_z_ins*, *mean_cross_accel_z_exp*)
- **Peak count of the breathing signal, three accelerometer axes** (*peaks*, *peaks_ins*, *peaks_exp*, *peaks_accel_x*, *peaks_accel_x_ins*, *peaks_accel_x_exp*, *peaks_accel_y*, *peaks_accel_y_ins*, *peaks_accel_y_exp*, *peaks_accel_z*, *peaks_accel_z_ins*, *peaks_accel_z_exp*)
- **Length of the breathing signal, three accelerometer axes** (*length*, *length_ins*, *length_exp*, *length_accel_x*, *length_accel_x_ins*, *length_accel_x_exp*)
- **Length ratio of the inspiration and expiration** (*lengthRatio*)
- **Area under the breathing signal** (*area*, *area_ins*, *area_exp*, *area_accel_x*, *area_accel_x_ins*, *area_accel_x_exp*, *area_accel_y*, *area_accel_y_ins*, *area_accel_y_exp*, *area_accel_z*, *area_accel_z_ins*, *area_accel_z_exp*)

In total, 19 features were engineered where 18 of them are being found for all inspirations, expirations and full breaths (except $lengthRatio$). This yields that in total there were 4 (3 axes and the breathing signal) * 18 (features) * 3 (full breath, inspiration, expiration) + 1 ($lengthRatio$) = 217 different features constructed.

The idea of using boxplots or other usual plotting methods was not generalizable which lead to another visual measurement designed specifically for the Ratios method described in Section 5.2. The reasoning for this new visualization technique is based on the differences in ratios between two classes. It is wanted to find features that present the opposite behaviour such that switching from one class to another shows either a much higher or much lower ratio. This can be done by the following steps:

1. Check whether three consecutive breaths have the same class.
2. Check whether the third breath has a different class than the previous three.
3. Save the ratio to normal class set if the class changes from obstructed to normal or set it to be in obstructed set if it is the other way around.
4. Plot with respect to each feature.

The previous steps yield plots in Figures 4.6, 4.7, 4.8, 4.9. To explain the steps above even more, one can say that it looks similar to the cyclic pattern of obstructions described in the Introduction. It is indeed similar by the fact that it is being tried to find the change happening when there is a sequence of obstructed breaths followed by a normal one. The switch between the last two is being saved. By carefully inspecting these plots 22 features were selected to be further analyzed. The results of this analysis can be seen in the second column of Table 4.1. Note that the following reasoning was applied during selection: most of the time some features have the same patterns, for example, the maximum of a breath is the same as the maximum of an inspiration. Taking this into account, it was chosen to take only one of these kind of features in order to maintain the uniqueness of them.

It can be noticed that none of the breathing signal features were selected. This proves the analysis made in Section 4.2 where the inconsistencies between the patterns of normal and obstructed breathing periods of were presented.

Now 22 features remained and one more step regarding the feature selection is performed. In Algorithm 7 the training of the Ratios model is being explained (more about this in Section 5.2.1) which involves setting the best upper and lower thresholds for each feature. This is done by taking thresholds which give the highest accuracy of classification of the training data.

For the last step in feature selection the Ratios model was trained on all breaths and the training accuracy for each feature was reported with respect to each patient and both patients together. The results can be seen in Table 4.1. Column ”Both patients” consists of training accuracies of the data which was combined out of patient 1 and patient 16 consecutively.

Thresholds for these percentages were taken to select a reasonable number of features for each patient and both patients together. For patient 1, patient 16 and both patients

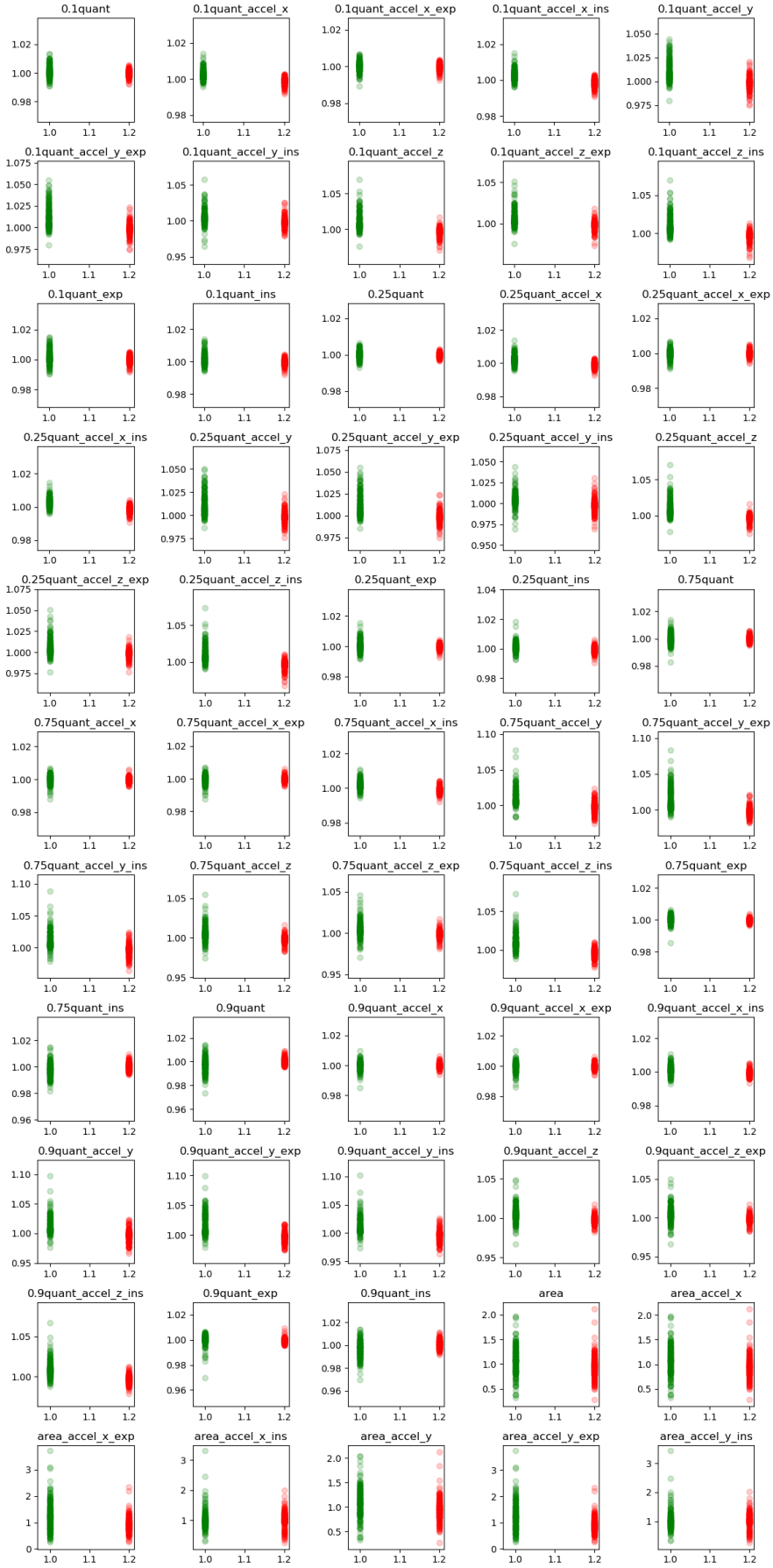

Figure 4.6: Plots of different features 1

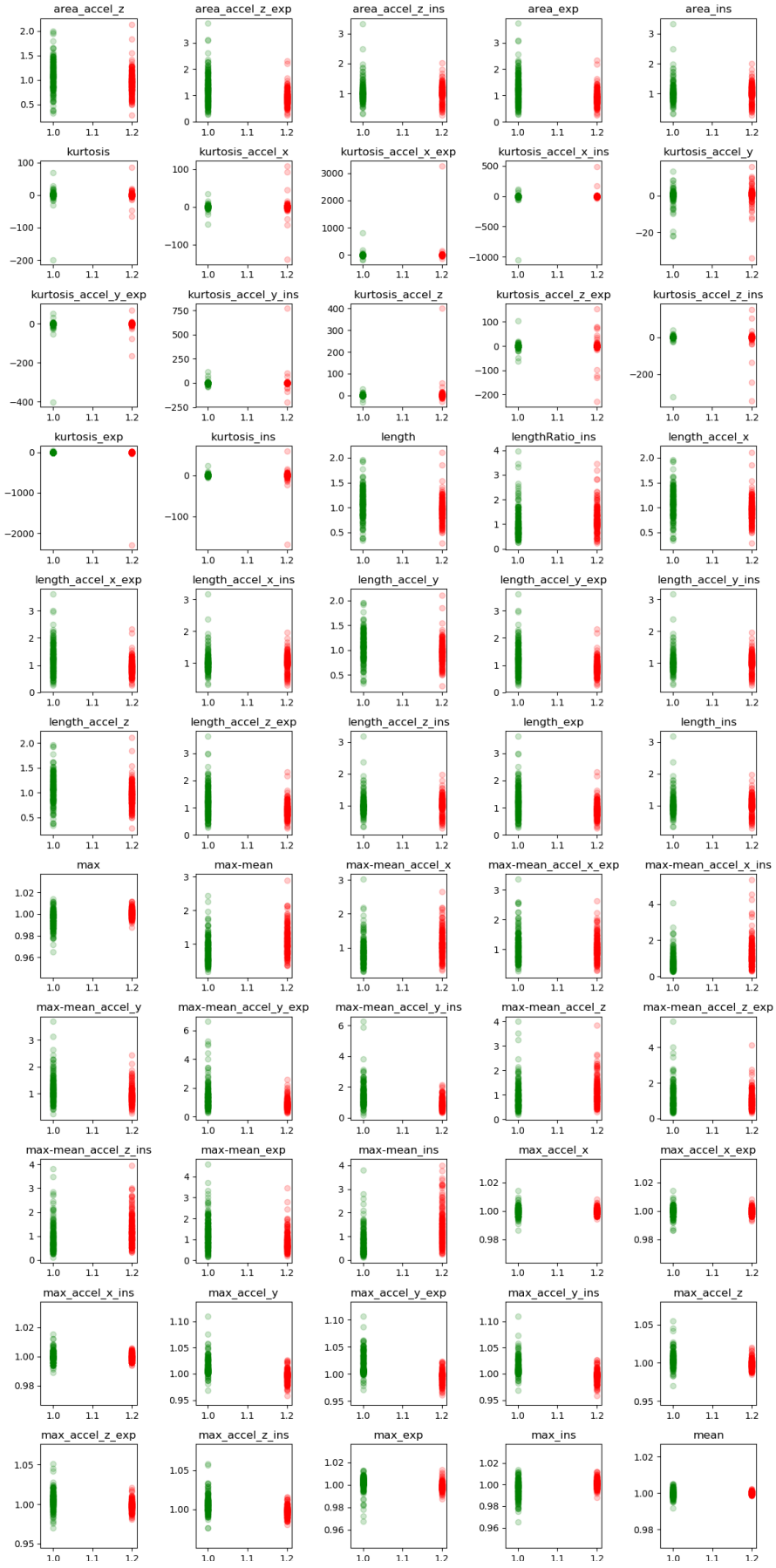

Figure 4.7: Plots of different features 2

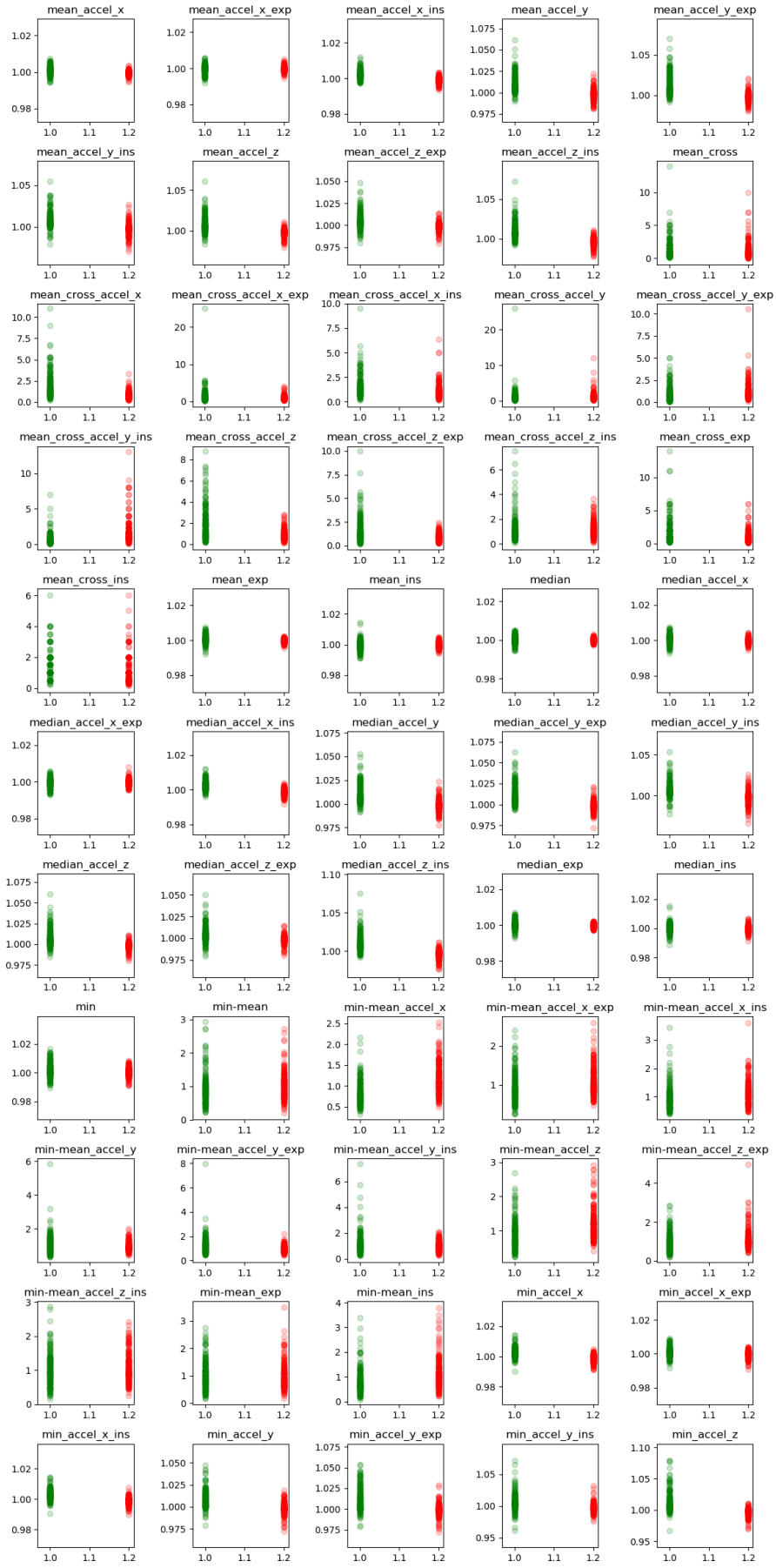

Figure 4.8: Plots of different features 3

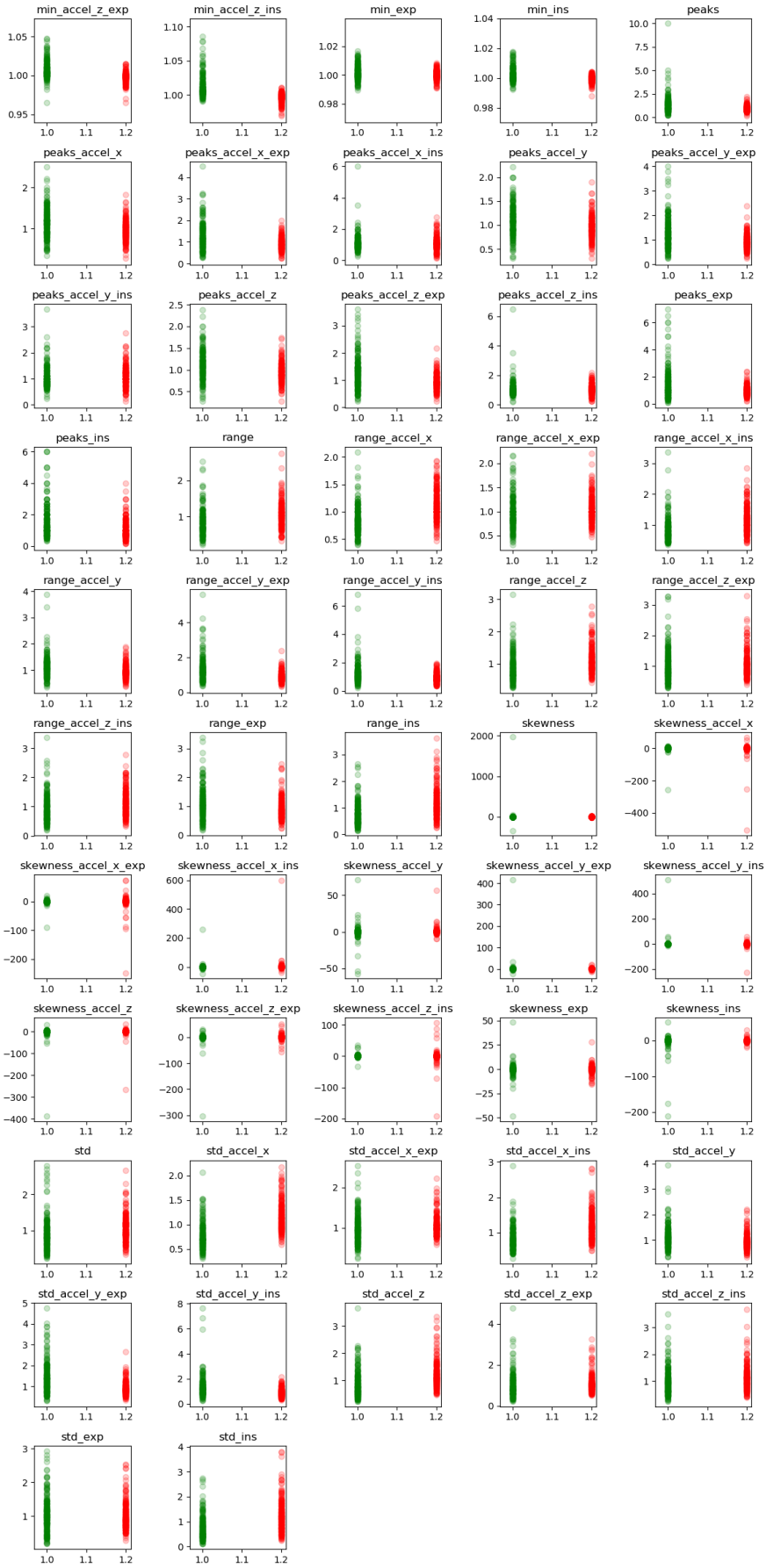

Figure 4.9: Plots of different features 4

Feature	Result	Both patients	Patient 1	Patient 16
$0.1quant\_accel\_x\_ins$	Lower for obstructed	86.69%	84.46%	88.91%
$0.1quant\_accel\_y$	Lower for obstructed	86.46%	88.85%	92.78%
$0.1quant\_accel\_z\_ins$	Lower for obstructed	88.43%	89.86%	91.2%
$0.25quant\_accel\_x\_ins$	Lower for obstructed	88.08%	84.80%	90.67%
$0.25quant\_accel\_y$	Lower for obstructed	86.92%	87.84%	91.37%
$0.25quant\_accel\_z\_ins$	Lower for obstructed	89.93%	90.88%	92.25%
$0.75quant\_accel\_y$	Lower for obstructed	80.09%	89.86%	87.32%
$0.75quant\_accel\_z\_ins$	Lower for obstructed	89.12%	90.54%	91.02%
$0.9quant\_accel\_y\_exp$	Lower for obstructed	83.22%	89.86%	91.02%
$0.9quant\_accel\_z\_ins$	Lower for obstructed	86.34%	86.82%	86.8%
max_accel_y	Lower for obstructed	79.17%	87.50%	86.09%
$mean\_accel\_y$	Lower for obstructed	84.61%	90.54%	91.37%
$mean\_accel\_x\_ins$	Lower for obstructed	87.50%	83.45%	90.32%
$mean\_accel\_z\_ins$	Lower for obstructed	90.51%	89.86%	92.43%
$median\_accel\_x\_ins$	Lower for obstructed	87.15%	83.78%	89.79%
$median\_accel\_y$	Lower for obstructed	83.91%	89.19%	90.32%
$median\_accel\_z\_ins$	Lower for obstructed	90.51%	91.55%	91.55%
$min - mean\_accel\_z$	Higher for obstructed	75.93%	80.07%	79.75%
$min\_accel\_x\_ins$	Lower for obstructed	84.84%	82.09%	88.20%
min_accel_y	Lower for obstructed	87.50%	87.84%	91.90%
$min\_accel\_z\_ins$	Lower for obstructed	88.89%	87.84%	91.37%
$std\_accel\_x\_ins$	Higher for obstructed	72.34%	83.11%	73.42%

Table 4.1: Ratios plots analysis

Patient 1	Patient 16	Both patients
0.1*quant_accel_z_ins* 0.25*quant_accel_z_ins* 0.75*quant_accel_z_ins* *mean_accel_z_ins* *median_accel_z_ins*	0.1*quant_accel_z_ins* 0.25*quant_accel_z_ins* 0.75*quant_accel_z_ins* *mean_accel_z_ins* *median_accel_z_ins*	0.1*quant_accel_z_ins* 0.25*quant_accel_z_ins* 0.75*quant_accel_z_ins* *mean_accel_z_ins* *median_accel_z_ins*
0.1*quant_accel_y* 0.9*quant_accel_y_exp* *mean_accel_y*	0.1*quant_accel_y* 0.9*quant_accel_y_exp* *mean_accel_y*	
	min_accel_y *min_accel_z_ins*	*min_accel_y* *min_accel_z_ins*
0.75*quant_accel_y*		
	0.25*quant_accel_y*	
		0.25*quant_accel_x_ins* *mean_accel_x_ins* *median_accel_x_ins*

Table 4.2: Best features

the thresholds were defined to be 87%, 91% and 88%, respectively. The best final features can be seen in Table 4.2. In each row it is presented where both patients or each individual patient are sharing the same best feature. Hence the first five features are shared between both patients and each individual patient, then the next three are representative only for each individual patient, next two - for both patients and patient 16, then cells include features that had good accuracies for patient 1, patient 16 and both patients, separately.

An interesting property can be noticed by analyzing Table 4.2. When considering each patient separately some features of y axis present high accuracies; however, when the patients' data is combined, only the features of z axis are shared between all three columns. This leads to a reasoning that each person has a unique way of abdomen movement with respect to y axis (look at Figure 2.1) while z axis which is responsible for up-and-down abdomen movements show general trends for both patients. Different sets of these best features in Table 4.2 are examined and results can be found in Section 5.2.4.

Chapter 5

Implementation and testing

5.1 Shapelets

The method which was considered when detecting different shapes of breaths was using time series shapelets. They are defined to be the representative subsequences of a number of possible classes. The whole implementation is based on L. Ye and E. J. Keogh work [30]. The goal of their research was to classify two different classes of leaves named Urtica dioica and Verbena urticifolia. One dimensional times series were produced by setting a middle point on a leaf and keeping a pointer on the edge moving it in one direction till the beginning is reached. By analyzing the time series representation of leaves, the difference between the joint of a leaf and stem was noticed which can be seen in Figure 5.1. The idea was to find all subsequences of different leaves classes and test which ones give the best separation which would be defined to be the representative shapes, or shapelets.

5.1.1 Definitions

In order to explain the procedure of finding the best shapelet which separates normal and obstructed breaths, some important variables must be incorporated first. The list with explanations defined for the breaths classification task can be found below.

- **TIME SERIES**. Let $T = t_1, ...t_m$ be the time series of m observed values corresponding to one breath sampled equally at a frequency of 32Hz where $t_i \in \mathbb{R}$.
- **SUBSEQUENCE**. Let $T = t_1, ...t_m$ be times series of length m, then a subsequence S of T is defined to be $S = t_p, ...t_{p+l-1}$ for $l \leq p \leq m - l + 1$, where l is the length of subsequence S.
- **SLIDING WINDOW**. For a time series T of length m and subsequence S of user chosen length l, all possible subsequences of T can be found by having a sliding window through T of the same size as the subsequence S (in this case l). In this way, subsequences S_p^l of T, where p defines the start of the sliding window and l the length of the subsequence, are extracted constituting to the full

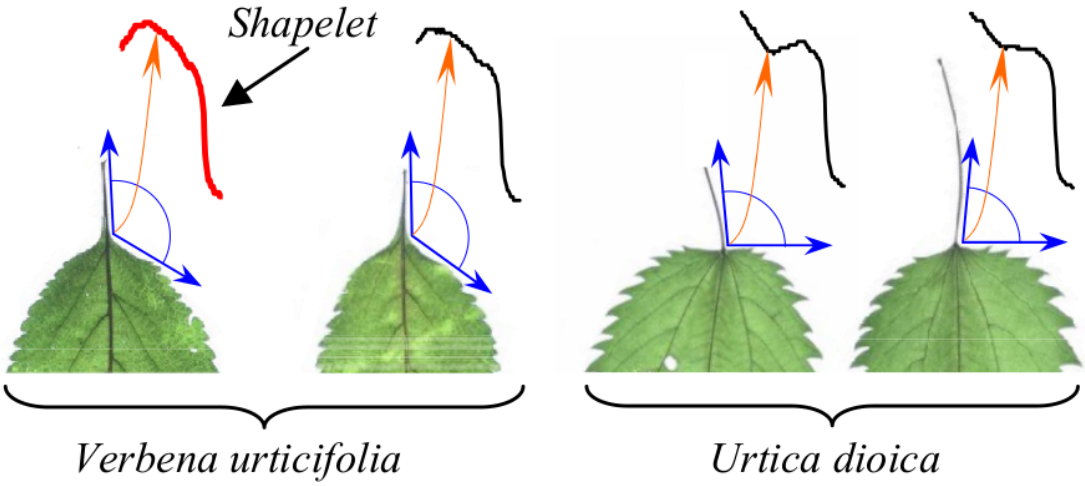

Figure 5.1: The difference between two classes of shapelets [30]

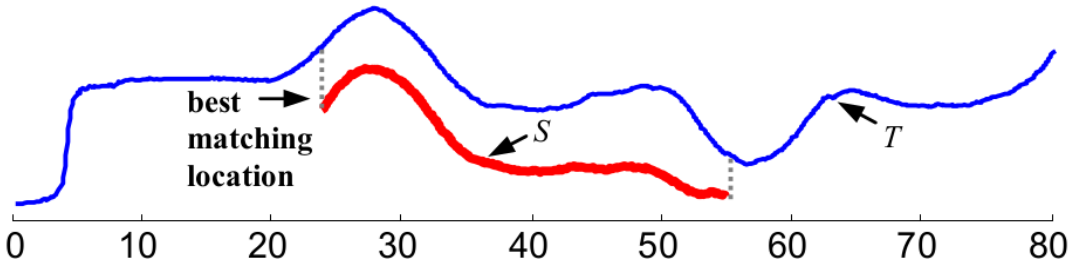

Figure 5.2: Distance between the time series and the subsequence [30]

subsequences set of T defined as

$$S_T^l = \{S_p^l \text{ of } T, \forall p \in [1, m-l+1]\}.$$

- **DISTANCE BETWEEN THE TIME SERIES**. Let the similarity measure between two time series T and R of the same length be $Dist(T,R)$. The output of $Dist(T,R)$ is defined to be $d \geq 0$ - the Euclidean distance between series T and R where $Dist(T,R) = Dist(R,T)$. This can be used for measuring the similarity between two subsequences of the same length as well.
- **DISTANCE BETWEEN THE TIME SERIES AND THE SUBSEQUENCE**. Let the similarity measure between the time series T and the subsequence S be called $SubsequenceDist(T,S)$. Note that the lengths of T and S might be different. However, it is always true that $l < m$, where l and m are the lengths of S and T, respectively. The output of $SubsequenceDist(T,S)$ is $d \geq 0$ which is the minimum distance from T to S defined as $min(Dist(S,S'))$, for $S' \in S_T^{|S|}$. In other words, d is the distance between S and T, where S and T match each other the best as it can be seen in Figure 5.2.
- **ENTROPY**. The metric which was chosen for checking how well the distances described above divide the two classes is based on the entropy. Let D denote a set of all time series given consisting of two possible classes A and B. Let $p(A)$ and $p(B)$ be the proportions of classes A and B in D, respectively. Then the

entropy I of D is defined to be:

$$I(D) = -p(A)log(p(A)) - p(B)log(p(B)). \tag{5.1}$$

Suppose we have a splitting of D into two subsets, D_1 and D_2. The information kept in the dataset after the split of D can be thought of as the weighted average entropy of both subsets. Let $f(D_1)$ and $f(D_2)$ be the fractions of objects in D_1 and D_2, respectively. Then the entropy after splitting I' is defined as:

$$I'(D) = f(D_1)I(D_1) + f(D_2)I(D_2). \tag{5.2}$$

- **INFORMATION GAIN**. Given a splitting sp of D into subsets D_1 and D_2, the entropy before and after the splitting is $I(D)$ and $I'(D)$, respectively. Note that the splitting rule is set to be the distance to a shapelet. Hence, the information gain which we choose to be the main metric for measuring the performance of the splitting is:
$$Gain(sp) = I(D) - I'(D). \tag{5.3}$$
Combining equations 5.2 and 5.3 the following is derived:
$$Gain(sp) = I(D) - f(D_1)I(D_1) - f(D_2)I(D_2). \tag{5.4}$$
Note a mistake in L. Ye and E. J. Keogh work [30], where the 3rd term in equation 5.4 is negative instead of positive.
- **OPTIMAL SPLIT POINT**. Since the dataset D consists of two classes A and B, namely normal and obstructed breaths, for a possible shapelet S, a distance threshold d_{th} is chosen to divide D into D_1 and D_2 such that the following is true: $SubsequenceDist(T_{1,i}, S) < d_{th}$ and $SubsequenceDist(T_{2,i}, S) > d_{th}$ for all objects $T_{1,i}$ and $T_{2,i}$ in D_1 and D_2, respectively. An optimal split point (OSP) is defined to be the distance threshold such that the following is true:
$$Gain(S, d_{OSP(D,S)}) \geq Gain(S, d'_{th}), \tag{5.5}$$
for any distance threshold d'_{th}.

5.1.2 Methodology

5.1.2.1 Brute-Force Algorithm

The brute force method for finding the shapelet follows Algorithm 1. All variables used in the algorithms can be found in Table 5.1.

The input to the function is the dataset D consisting of all breaths, corresponding labels Y and maximum $maxl$, minimum $minl$ lengths of a shapelet.

Firstly, all possible shapelets of lengths in the interval $[minl, maxl]$ are found using function $generate(D, maxl, minl)$ defined in Algorithm 2. This function loops through each possible length of a shapelet followed by the iteration through the time series in

Variable	Definition
D	Dataset of all breaths.
Y	Labels corresponding to the dataset D.
$maxl$	Maximum length of a shapelet.
$minl$	Minimum length of a shapelet.
T	Time series of one breath.
l	Incrementing variable between $minl$ and $maxl$.
S	Candidate shapelet.
X	Minimum distances between S and each T in D.
D_1	A subset of D after the split corresponding to class A (look at definition for **ENTROPY** and Equation 5.2).
D_2	A subset of D after the split corresponding to class B (look at definition for **ENTROPY** and Equation 5.2).
$Y1$	A subset of Y after the split corresponding to class A - labels of D_1.
$Y2$	A subset of Y after the split corresponding to class B - labels of D_1.
pA	The proportion of class A in Y.
pB	The proportion of class B in Y.
$pA1$	the proportion of class A in $Y1$.
$pB1$	the proportion of class B in $Y1$.
$pA2$	the proportion of class A in $Y2$.
$pB2$	the proportion of class B in $Y2$.

Table 5.1: Definitions of variables

Algorithm 1 Brute force algorithm for finding the shapelet

```
1:  procedure FINDSHAPELET(D, maxl, minl, Y)
2:      candidates ← generate(D, maxl, minl)
3:      bsf_gain ← 0
4:      bsf_shapelet ← []
5:      for S in candidates do
6:          gain, model = checkCandidate(D, S, Y, bsf_gain)
7:          if gain ≥ bsf_gain then
8:              bsf_gain = gain
9:              bsf_shapelet = S
10:             bsf_model = model
11:         end if
12:     end for
13:     return bsf_shapelet, bsf_model
14: end procedure
```

Algorithm 2 Finding all possible subsequences of a given dataset

```
1:  procedure GENERATE(D, maxl, minl)
2:      pool ← []
3:      l = maxl
4:      while l ≥ minl do
5:          for T in D do
6:              pool+ = shapeletsLength(T, l)
7:              l− = 1
8:          end for
9:      end while
10:     return pool
11: end procedure
```

Algorithm 3 Finding all possible fixed-length subsequences of a given time series

```
1: procedure SHAPELETSLENGTH(T, l)
2:     lshapelets ← []
3:     for j in indices of T do
4:         if j + 1 ≤length of T then
5:             lshapelets.append(T[j : j + 1])
6:         end if
7:     end for
8:     return lshapelets
9: end procedure
```

the dataset and uses another function $shapeletsLength(T,l)$ (see Algorithm 3) to get all the candidate shapelets of time series T in D of length l.

After all candidate shapelets are generated, the loop iterating each of those is executed in lines 5-12 of Algorithm 1. The main goal of this loop is to check which candidate shapelet generates the best information gain. To find the information gain of splitting based on a particular candidate shapelet S a method $checkCandidate(D,S,Y)$ is used. In Algorithm 4 the distance between a candidate shapelet and a particular time series in the dataset D is found using method $subsequenceDist(T,S)$ in Algorithm 5 where the definitions of a sliding window and the distance between the time series and the subsequence from Section 5.1.1 are being implemented. Note that the function is using Euclidean distance for the similarity measure with an optimization technique of "early abandon" described in Section 5.1.2.2.

Algorithm 4 Getting an information gain given by splitting with a candidate shapelet

```
1:  procedure CHECKCANDIDATE(D, S, Y, bsf_gain)
2:      X ← []
3:      for j in indices of D do
4:          X.append(subsequenceDist(D[j], S))
5:          min_dist ← min(X)
6:          max_dist ← max(X)
7:          classA_count ← the number of class A objects in D disregarding the first
              j objects
8:          classB_count ← the number of class B objects in D disregarding the first
              j objects
9:          X_pruning ← a list of X followed by min_dist and max_dist appearing
              classA_count and classB_count times, respectively
10:         Y_pruning ← a list of the first j elements from Y followed by class A and
              class B labels classA_count and classB_count times, respectively
11:         if calcInfoGain(D, X_pruning, Y_pruning)[0] < bsf_gain then
12:             return (-infinity, False)
13:         end if
14:     end for
15:     return calcInfoGain(D, X, Y)
16: end procedure
```

Finally, following Algorithm 4 when the minimum distances X between a particular candidate shapelet and all time series in the dataset are found using $subsequenceDist(T,S)$, the information gain can be calculated using $calcInfoGain(D,X,Y)$. A simple decision tree of depth 1 is being used to find the split threshold d_{th} as described in Section 5.1.1. Algorithm 6 presents the training of a decision tree which corresponds to finding the best threshold and calculating the information gain which is passed through all the functions until it reaches $findShapelet$. The error handling in line 11 includes checking whether any of the probabilities $pA, pB, pA1, pB1, pA2, pB2$ (look at Table 5.1) are zero and setting those to be equal to 1 for logarithms in the formulas in lines 12-15 to be equal to 0, in other words, no information gain. Finding the best information gain

Algorithm 5 Finding the minimum distance between a candidate shapelet and a time series in the dataset

```
1:  procedure SUBSEQUENCEDIST(T, S)
2:      mini ← infinity
3:      stop ← False
4:      i ← 0
5:      while i+length of S ≤length of T do
6:          sum_dist ← 0
7:          Ti ← T[i : i+length of S]
8:          for j in indices of S do
9:              sum_dist+ = (Ti[j] − S[j])^2
10:             if sum_dist ≥ mini then
11:                 stop ← True
12:                 break
13:             end if
14:         end for
15:         if stop = False then
16:             mini = sum_dist
17:         end if
18:         i+ = 1
19:     end while
20:     return mini
21: end procedure
```

is performed in lines 7-10 of a function $findShapelet(D.maxl, minl, Y)$ described in Algorithm 1.

Algorithm 6 Calculating the information gain

```
1:  procedure CALCINFOGAIN(D, X, Y)
2:      model ← decision tree of depth one
3:      fit model with X and Y
4:      divide Y into Y1 and Y2
5:      error handling when probabilities of entropies are zeros
6:      ID = −pA ∗ math.log(pA) − pB ∗ math.log(pB)
7:      ID1 = −pA1 ∗ math.log(pA1) − pB1 ∗ math.log(pB1)
8:      ID2 = −pA2 ∗ math.log(pA2) − pB2 ∗ math.log(pB2)
9:      gain = ID − (len(Y1)/len(Y)) ∗ ID1 − (len(Y2)/len(Y)) ∗ ID2
10:     return gain, model
11: end procedure
```

5.1.2.2 Optimization

1. Early abandon. As mentioned in the last section, lines 8-17 of Algorithm 5 show an optimization technique called "early abandon" [33]. The main idea of this method is to prune subsequences produced by a sliding window which partial lengths exceed the already existing minimum length between a particular candidate shapelet and a subsequence of the time series (sliding window). Line 9 of Algorithm 5 is calculating the Euclidean distance for each point between a candidate shapelet S and a moving window T_i of T. Since only the minimum distance matters we can stop executing line 9 for a particular sliding window T_i if *sum_dist* exceeds the already known minimum distance *mini*.

2. Entropy pruning. Another optimization technique implemented in lines 5-12 of Algorithm 4 for a faster performance. The idea behind this involves pruning a candidate shapelet by putting an upper bound on the information gain. In the loop the maximum and minimum distances of the current available set are found and the information gain is calculated for the best possible outcome. Obviously, the best way would be if the rest of the objects in D are correctly classified. Hence we append the minimum and maximum distances appearing the number of times classes A and B appear in the rest of D, respectively (disregarding the first j objects because we already have the minimum distances in X). If the best outcome information gain is lower than the current best one, the consideration of this candidate shapelet is done. Since it is fast to get the information gain (it is just a decision tree of depth 1 and some easy calculations taking constant time), this helps to reduce the number of distance calculations necessary for finding the shapelet.

5.1.3 Results

The goal of the Shapelets method is to find some representing shapes of signals similar as described in Section 4.1. Since different classes do not exactly present a clear difference in shapes, an attempt of trying to find the ones that can separate two classes the best will be made. All five time series, namely accelerometer axes x, y, z, breathing signal and cannula values were used for trying to find the best shapelet. A rolling mean of 5 was used in order to reduce noise and smoothen the accelerometer values. The data is split into the training and validation sets with a ratio of 4:1.

First of all, the method described in Section 5.1 is considered without any modifications. Only the inspirations are taken as in Section 4.1 since most of the breathing obstructions happen when inhaling. Note that using accelerometer axes when calculating the distance would be insensible since it is known from Section 4.2 that they tend to scale after some time. Hence, only the comparison between the breathing signal and nasal cannula values will be considered in this case. By looking at the distribution plot of lengths of both patients' inspirations in Figure 5.3 it can be seen that most of the inspirations have length of around 40-50. In order to delete breaths which memory marks are poorly identified or the ones which are too short it was decided to take only those breaths which have the length of inspiration and expiration greater than 35. Then the maximum and minimum shapelet lengths for Algorithm 1 were chosen to be 35 and 20, respectively. This decision was based on the fact that the length of a shapelet cannot exceed any length of a breath in dataset D which is 35. The minimum length was taken to be 20 such that it would be long enough to represent a pattern. The results can be seen above the black line in Figure 5.4 where the shapelets found are plotted and results presented with respect to each signal and patient.

It can be seen that the cannula obstruction shapes were found as expected, yielding great accuracies for each patient separately and together. By looking at the top right shapelet in Figure 5.4 which represents the shapelet found for both patients and showing the accuracy of 83.83% one can argue that this curve found resembles the class 2 shape defined by T. Aittokalio et al. [14] which can be visualized in Figure 3.1. However, the aim of this project is not to use the cannula signal but other signals produced by RESpeck monitor. When analyzing the second row of Figure 5.4, it is noticeable that the breathing signal does not perform very well in separating two classes, namely normal and obstructed. For patient 16, it was able to find a shapelet which proposed a 74.49% accuracy; however, for patient 1 and both patients together, results yield only 59.4% of correctly classified validation samples. This shows that using the distance measure with the breathing signal should not be a way to go when trying to distinguish the obstructions.

Now some modifications were made to the algorithm in order to apply the Shapelets method more wisely while facing the problem of scaling as mentioned in the last paragraph. In this way, all accelerometer axes can be incorporated in the shapelets analysis. The difference is that instead of using the Euclidean distance, Pearson correlation was calculated. The idea is to maximize it and find shapelets which separate two classes the best based on the correlation of the shapes. As noted in Section 4.1 some axes represent a faster increase or decrease corresponding to obstruction which means that an

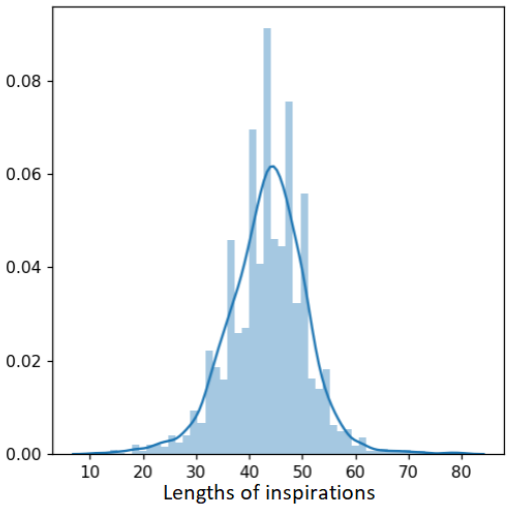

Figure 5.3: Distribution of lengths of inspirations

attempt in finding the linear correlation between a particular shapelet and other inspirations can be made. The correlation coefficient is not influenced by the scaling which makes the accelerometer values suitable. Hence, Algorithm 5 was slightly modified to maximize the Pearson correlation. The resulting shapelets can be seen in Figure 5.4 on the bottom of the line. Note that it would be unreasonable to calculate the Pearson's correlation coefficient for cannula and breathing signals since during the inspiration they are not linear. Hence, only the three accelerometer axes are taken when using the Pearson's correlation coefficient.

By looking at the accelerometer x (*accel_x*) signal shapelets found it can be noted that when two patients are considered separately, those curves are quite similar giving the idea that they might present the same pattern of a decrease as it can be noticed in the third row of Figure 5.4. However, the accuracies are quite different for patient 1 and patient 16 separately, yielding to 62.32% and 86.39%, respectively. Note that the shapelet found for both patients (the rightmost plot on the third row) shows a completely different pattern, concluding that accelerometer x signal can only be used for patient 16 but the performance on both patients and patient 1 is not good enough to use for the classification purposes. Now focus on accelerometer y axis which results are presented on the fourth line of Figure 5.4. It can be noticed that there is a general trend of an increase and the accuracies found are just below 70%. Meanwhile, accelerometer z axis is showing the best results, as expected (since it corresponds to up-and-down movement as in Figure 2.1). The shapelets found for patient 1 and 16 are quite similar which means it is a generalized signal which shows similar patterns to different patients. The accuracies for both patients separately show 77.90% and 85.37%. However, it can be noted that the shapelet found for both patients together differs a bit from when these patients were considered separately. The total accuracy is 70.65% which is much better than the ones reported for other signals.

Another improvement that was implemented is scaling every breath to the same interval and resampling to the median length similarly as in Section 4.1. Note that now

the algorithm seeks to find a subsequence of time series corresponding to inspirations while in Section 4.1 the naive reasoning of taking the mean of all same class shapes was used. Even though these two are slightly different problems, it is being hoped that the shapelets found by the algorithm are similar to the ones in Section 4.1 which would show the representativity of the shape of a particular signal. The results using this method with both Euclidean distance and Pearson's correlation coefficient measures can be seen in Figure 5.5 on the top and bottom of the line, respectively.

First of all, the distance measure will be discussed. For the cannula signal each patient separately show the shapelets of obstructions since the flatenning of the waveform appears. However, when both patients are taken together, it can be argued that the separating shapelet found corresponds to the normal shape (class 1 in Figure 3.1). Again, cannula signal is not the one of interest; hence, other signals will be considered now. In Figure 5.5 it can be seen that the breathing signal shows some good results for each patient separately and combined data (both patients together) as well presenting 78.01%, 80.71% and 73.69%, respectively. Accelerometer x and y axes present quite poor performance resulting in very differing shapelets. Again, accelerometer z axis shows the highest results compared with other axes and present 79.43%, 79.35% of accuracy for each patient individually and a combined accuracy of 77.08%. Note that the shapelets found for the best signals, namely the breathing signal and accelerometer z axis are differing slightly between patients but showing some similar pattern yielding good accuracies.

Now the Pearson's correlation coefficient is considered to be the measure for the algorithm. All three accelerometer axes shapelets with their results are found below the black line in Figure 5.5. Note that x axis is not representative showing completely different curves for each patient individually and both of them together. Y axis presents a similar trend of an increase between each patient and the combined data; however, the accuracies reported are too low for this axis to be considered as representative. By looking at the last row of Figure 5.5 it can be noticed that z axis is presenting the best results using the Pearson's correlation coefficient when comparing with other two axes. Note that the shapelets found are the same when using the Euclidean distance measure. Even though the curves are not entirely identical between each patient and both of the together, some similar patterns can be noticed leading to 76.60%, 79.08% and 76.92% accuracies for patient 1, patient 16 and both patients together, respectively.

It was found that the accelerometer z axis axis provides with the best results, namely 77.08% of both patients accuracy. It is intuitive because of the reason that this axis corresponds to up-and-down movement of the abdomen. Note that accelerometer x and y axes did not show great results as expected because of the body shapes discussion in Section 4.1 leading to different shapes of accelerometer values when the body position changes even slightly. However, more research could be done in analyzing the effect of body shapes and positions onto the accelerometer axes which might bring up an idea that several shapelets and groupings could be defined as it is suggested in Section 6.1.

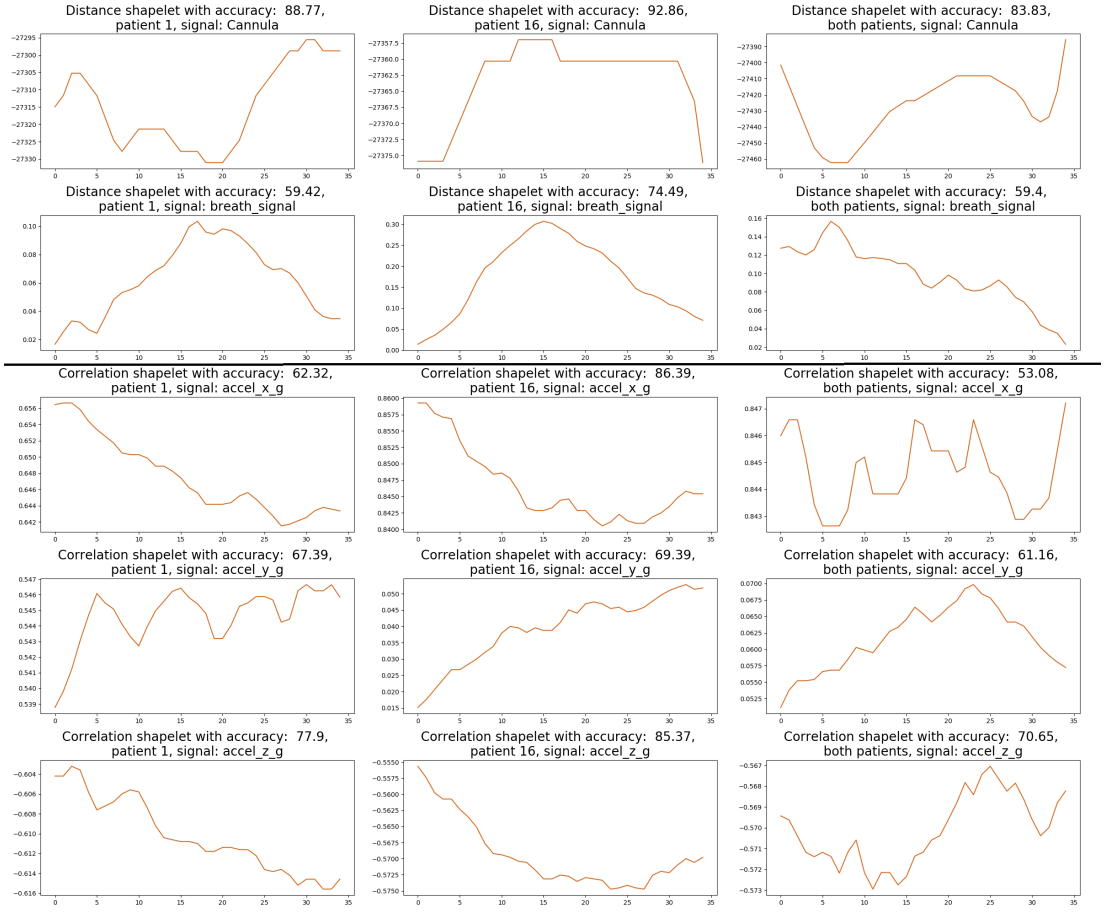

Figure 5.4: Shapelets with respect to each signal

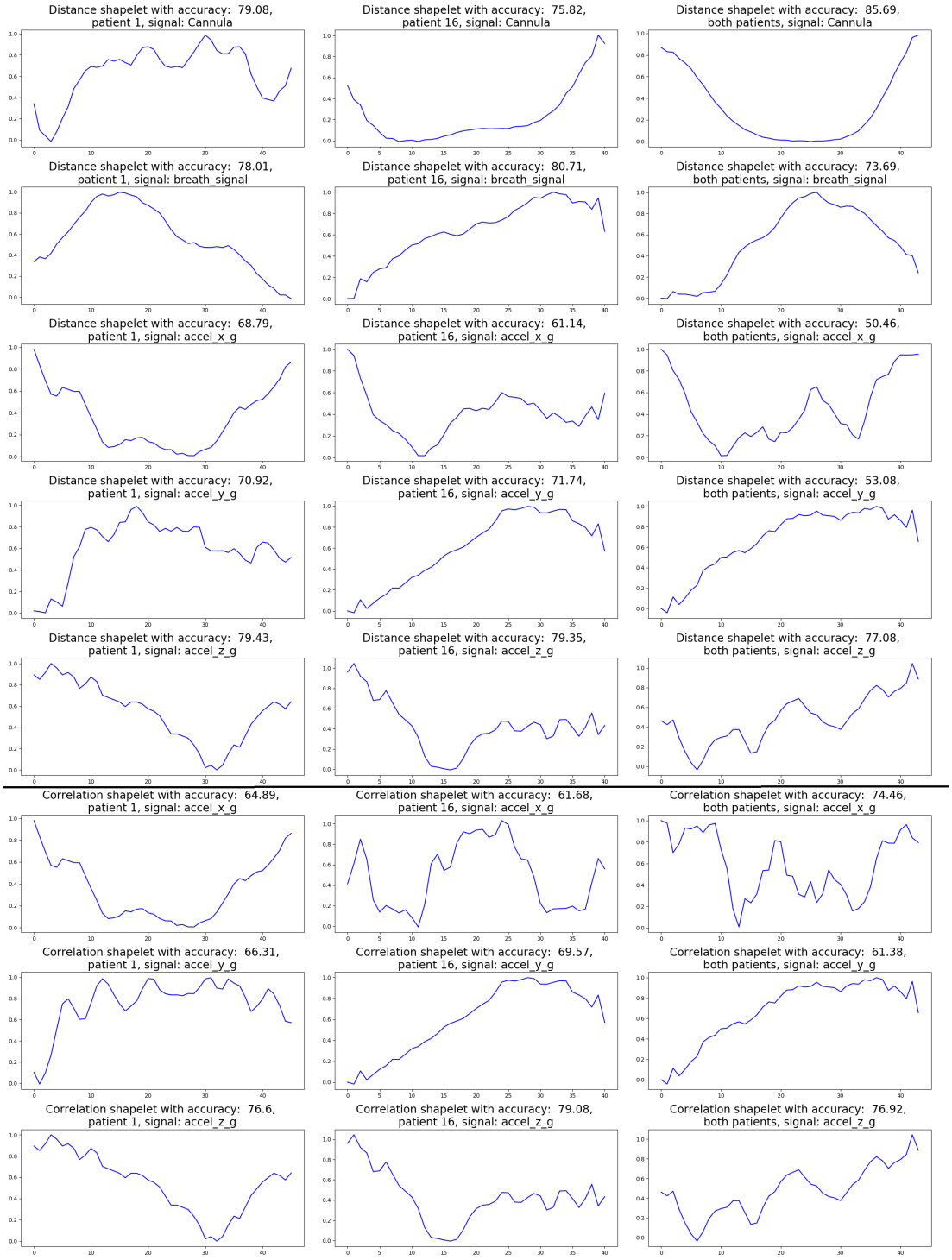

Figure 5.5: Shapelets with respect to each signal where inspirations were scaled and resampled

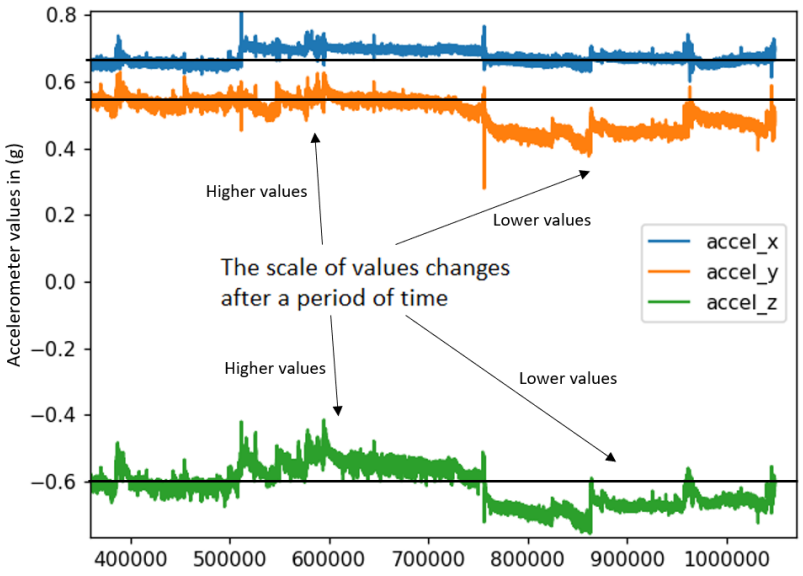

Figure 5.6: Changes in values after a long period of time

5.2 Ratios model

A new algorithm was designed and implemented to classify sequences of breaths while using ratios of features engineered in Section 4.4. The goal of this model is fixing the best lower and upper thresholds for ratios between a sample and a previous sample for each feature and looking for a large enough change from one breath to another with respect to each feature. Finding the prediction involves taking the median of all separate predictions made by each feature.

Note that the idea of this project is to find a way of continuously identifying the quality of breathing of a person which proposes that the model should be invariant of changes appearing in scaling after a long time period. An example of this can be seen in Figure 5.6 where breathing towards the end appears hours after the breaths in the beginning. Noticeable changes in scaling are apparent making the usual machine learning models useless in this case. One more thing, if filtering (such as Butterworth) was applied to the accelerometer values, all the scaling insights in Section 4.4 would be lost.

Additionally, the changes of features are local as you can see in Figure 5.7. Red and green colored signals correspond to obstructed and normal breaths, respectively. It is noticeable that the second period of obstructions gives much smaller breathing signal values; however, locally they are larger than the ones of the normal breathing which leads to breaths being obstructed.

5.2.1 Methodology

The training Algorithm 7 consists of the following steps:

1. The initial variables are being introduced. In Algorithm 7 the initialization of

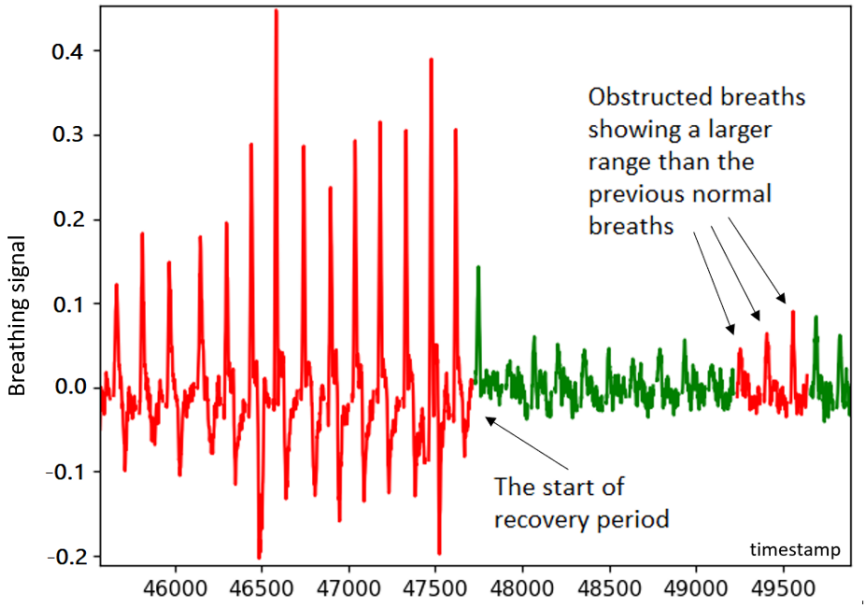

Figure 5.7: Local changes in classes

low_obs was done corresponding to the features which were selected to be the ones that showed lower values for obstructed breathing compared with the normal one using the plots in Figures 4.6, 4.7, 4.8, 4.9, respectively. These features include the ones from Table 4.1 where the second column indicates: Lower for obstructed.
Features in a list $selected\_feat$ are taken from Section 4.4 where the final engineered features are described.
In addition to this, variables X_train and y_train define the training set, constituting of ratios between each consecutive features, with their corresponding true labels, respectively.

2. The best maximum and minimum thresholds for changing the class are found in lines 6-39 of Algorithm 7. The first thing done is defining the possible thresholds sets for each feature. This can be done by visualizing the distribution plots and checking the deviation between values. The distribution plot for each feature can be found in Figure 5.8. It is evident that some features like $0.1quant\_accel\_z\_ins$ span their ratios in the interval [0.975, 1.025] while for others like $median\_accel\_x\_ins$ the range of values is much smaller. That is why the decision was made to set the intervals for the thresholds to be [5% quantile, 95% quantile] of each feature. In this way, the threshold intervals are set to be based on that feature's values, so larger range of them will correspond to a larger possible thresholds interval, and vice versa. Then depending on whether the feature is in *low_obs* or not the classification is being made. There are five possible cases of label switching:
    - If the ratio of current breath is greater than the upper threshold max_the and the feature is in a set *low_obs*, the prediction is "normal". The reason why that is the case is because the current breath has much higher values than the previous one and since the feature is in *low_obs* higher values of it

correspond to class ”normal”.

- If the ratio of current breath is greater than the upper threshold *max_the* and the feature is not in a set *low_obs*, the prediction is ”obstructed”. The reason why that is the case is because the current breath has much higher values than the previous one and since the feature is not in *low_obs* higher values of it correspond to class ”obstructed”.
- If the ratio of current breath is less than the lower threshold *min_the* and the feature is in a set *low_obs*, the prediction is ”obstructed”. The reason why that is the case is because the current breath has much lower values than the previous one and since the feature is in *low_obs* lower values of it correspond to class ”obstructed”.
- If the ratio of current breath is less than the lower threshold *min_the* and the feature is not in a set *low_obs*, the prediction is ”normal”. The reason why that is the case is because the current breath has much lower values than the previous one and since the feature is not in *low_obs* lower values of it correspond to class ”normal”.
- If the ratio is in-between *max_the* and *min_the*, the prediction is not changed from the previous one, so it carries the same prediction until the change in ratios is big enough (outside the interval *max_the* and *min_the*).

3. For each feature, steps above are being made also taking into account some exceptions/improvements mentioned in lines 26-27.
   First of all, for checking the exceptions, two lists have to be maintained. The first one keeps track of all the previous predictions being made while the second one consists of the ratios between features of breaths with the features of two preceding breaths. The following are the cases where the algorithm described in Step 2 can go wrong.
   - **Slowly decreasing values in cannula signal leading to obstruction**. Every ratio is not big or small enough (depending on whether it is in a list *low_obs*) for a breath to be switched to a different class. That is why some knowledge of preceding breaths is taken into account. This exception involves checking whether the previous two predictions and the current prediction (derived in Step 2) were classified as normal. If that is the case another two checks are being carried out:
     - If the ratio of the current feature and the one of two preceding breaths is greater than the upper threshold *max_the* and that feature is not in *low_obs*, then the prediction is switched from normal to obstructed.
     - If the ratio of the current feature and the one of two preceding breaths is smaller than the lower threshold *min_the* and that feature is in *low_obs*, then the prediction is switched from normal to obstructed.

     In this case, we check that the obstruction becomes more apparent by looking not only at the previous breath but the one before that one as well and the problem is being solved by those 2 steps above.
     An example of this kind of behaviour can be seen in Figure 5.9a. If three breaths marked as 1, 2, 3 are considered, the behaviour of this exception can be explained using the comparison between z axis and cannula signal. First of all, by looking at the cannula signal one can deduce that breaths 1 and 2

are normal and the 3rd one is obstructed because of the obvious flattening in the cannula signal. Another important thing that must be mentioned is that in Figure 5.9a axis z values are lower for obstructed breaths and higher for the normal ones. Moving back to Figure 5.9a it can be noticed that by considering values of axis z the change is not major: values for breaths 1, 2 and 3 are decreasing slowly similarly as the cannula inspiration range. As an example consider feature - the mean of axis z. Now the ratios method would not find any noticeable changes between 1 and 2, 2 and 3 breaths and all of those will be left as the previous class; hence, 1, 2 and 3 will be classified as normal. This is the place where the exception resolves the situation. In this case, since 1, 2 and 3 are marked as normal the comparison of the ratio of means between breaths 3 and 1 will also be made and a noticeable change will be inspected. Finally, the class of breath 3 will be changed to obstructed since the comparison of breaths 3 and 1 showed a big enough change in their mean values.

- **One accidental normal breath in a row of obstructed breaths**. This exception checks if a breath is classified as normal and the preceding two breaths were predicted as obstructed. If that is the case, another two checks are being made:
  - If the ratio of the current feature and the second previous one is greater than the lower threshold *min_the* and that feature is not in *low_obs*, then the prediction is switched from normal to obstructed. The reasoning behind this is that if the ratio of the current feature and the one of two preceding breaths does not cross the lower threshold *min_the* then it should not switch the prediction. Hence, the class of the two preceding breaths was obstructed which means the same class is being kept for the current breath as well.
  - If the ratio of the current feature and the second previous one is smaller than the upper threshold *max_the* and that feature is in *low_obs*, then the prediction is switched from normal to obstructed. The idea behind this is that if the ratio of the current feature and the one of two preceding breaths does not cross the upper threshold *max_the* then it should not switch the class. Hence, the class of the two preceding breaths was obstructed which means the same class must be kept for the current breath as well.

  An example of this case can be seen in Figure 5.9b. As before lower mean values of axis z lead to breaths being obstructed and higher means being normal. In this case, breaths 1-3 are obstructed because of noticeable lower flow of air and truncations in the cannula signal. Now the ratios method would find that breaths 1-2 are obstructed since there is a noticeable change between the 1st breath and the preceding. It is noticeable that breath 2 has the lowest mean value out of these 3 obstructed breaths and breath 3 would be predicted to be normal since there would be quite a significant change in ratios of features of breaths 3 and 2. However, the exception checks whether the comparison between breath 3 and 1 also presents a noticeable change in means which would not be the case. Hence, the class would be

switched from normal to obstructed.

- **One accidental obstructed breath in a row of normal breaths**. This exception checks if a breath is classified as obstructed and the preceding two breaths were predicted as normal. If that is the case, another two checks are being made:
  - If the ratio of the current feature and the second previous one is greater than the lower threshold *min_the* and that feature is in *low_obs*, then the prediction is switched from obstructed to normal. The reasoning behind this is that if the ratio of the current feature and the one of two preceding breaths does not cross the lower threshold *min_the* then it should not switch the prediction. Hence, the class of the two preceding breaths was normal which means the same class is being kept for the current breath as well.
  - If the ratio of the current feature and the second previous one is smaller than the upper threshold *max_the* and that feature is not in *low_obs*, then the prediction is switched from obstructed to normal. The idea behind this is that if the ratio of the current feature and the one of two preceding breaths does not cross the upper threshold *max_the* then it should not switch the class. Hence, the class of the two preceding breaths was normal which means the same class must be kept for the current breath as well.

  An example of this case can be seen in Figure 5.9c. Consider that lower mean values lead to a breath being obstructed and higher ones - normal. Here, breaths 1, 2 and 3 are all normal. However, the ratios method would find that only breaths 1 and 2 are not obstructed since the mean values of previous breaths are much lower but would fail to predict the 3rd one as normal. The reason behind this is that breath 2 can be defined as ”more normal” which means it has much higher mean values than the previous normal breaths. In this way, breath 3 has much lower mean than the preceding breath which leads to it being predicted as obstructed. This exception checks the ratio between not only the preceding breath but the one before as well. Hence, the ratio of means between breaths 3 and 1 would not show a significant change in the mean value which means that the class of breath 3 would be corrected to be normal.

Combining steps 2 and 3 the best thresholds are found and stored for each feature and the training of the model is done.

5.2.2 Optimization

For improving the performance with respect to time an optimization technique was implemented. During the training every time a sample was classified incorrectly, the number of these misclassified numbers was kept. If at any point of execution in lines 6-39 of Algorithm 7 the number of wrongly identified tuples was greater than the best one already found, this selection of *min_the* and *max_the* was discarded and another combination of thresholds was tested.

Algorithm 7 Ratios algorithm

```
1: procedure RATIOS
2:     selected_feat ← Features which were selected to be representative
3:     low_obs ← Features for which obstructed breaths tend to have lower values than normal breaths
4:     X_train ← Ratios: features divided by previous features of the training data
5:     Y_train ← Correct classes for the training data
6:     for feature in selected_feat do
7:         max_set ← 100 values of possible maximum thresholds
8:         min_set ← 100 values of possible minimum thresholds
9:         for max_the in max_set do
10:            for min_the in min_set do
11:                for ratio in X_train do
12:                    if ratio > max_tre then
13:                        if feature in low_obs: then
14:                            pred ← 0
15:                        else
16:                            pred ← 1
17:                        end if
18:                    end if
19:                    if ratio < min_tre then
20:                        if feature in low_obs: then
21:                            pred ← 1
22:                        else
23:                            pred ← 0
24:                        end if
25:                    end if
26:                    if exception then
27:                        change pred
28:                    end if
29:                    count ← No. of all correctly classified samples
30:                    count_cyclic ← No. of correctly classified cyclic samples
31:                    if count_cyclic is better than the previous best cyclic count then
32:                        save the best thresholds
33:                    end if
34:                    if count_cyclic is equal to the previous best cyclic count and
                         count is better than the best previous count then
35:                        save the best thresholds
36:                    end if
37:                end for
38:            end for
39:        end for
40:    end for
41:    close;
42: end procedure
```

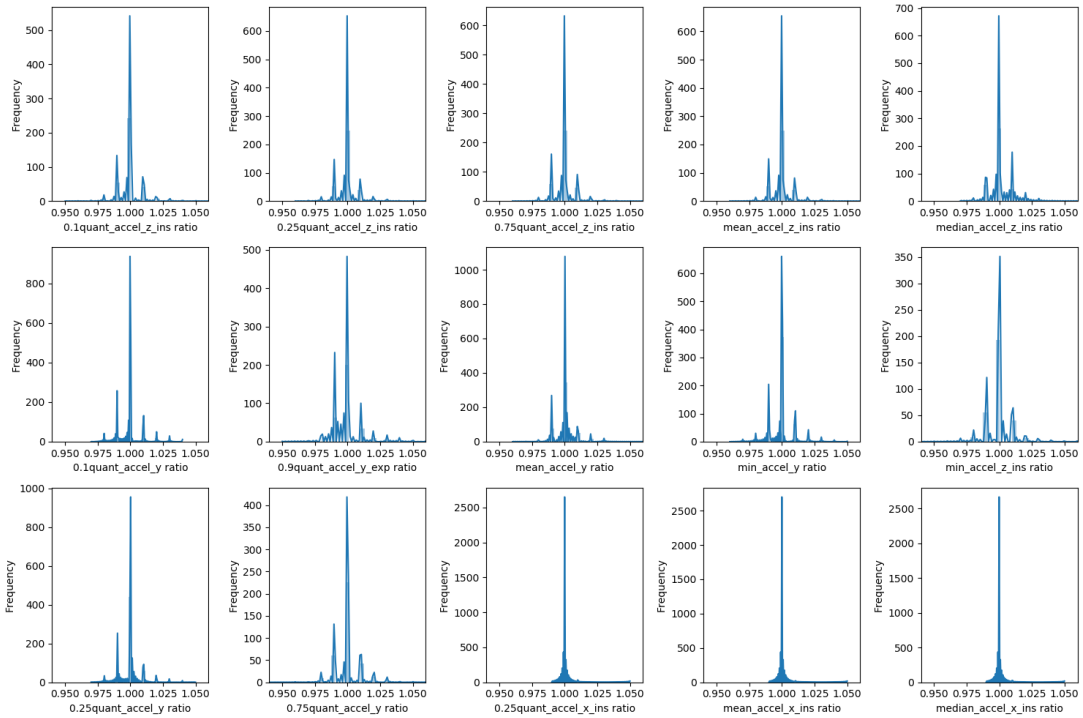

Figure 5.8: Distribution plots of the chosen features

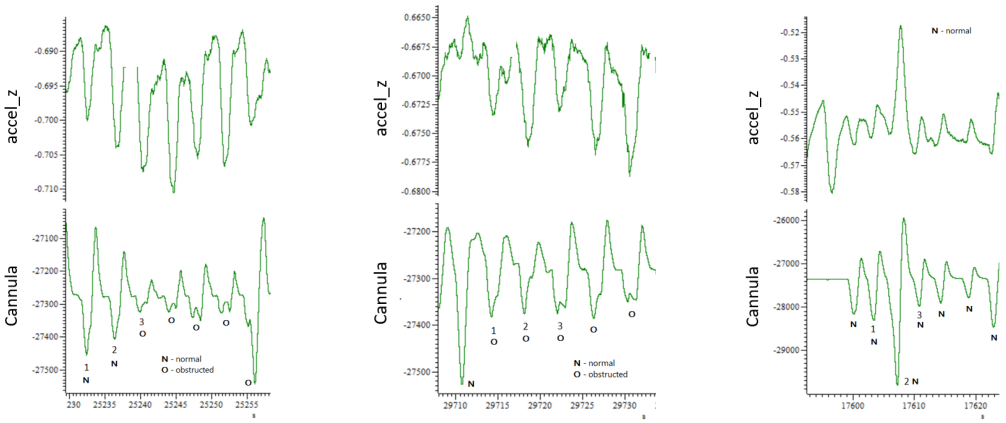

(a) Slowly decreasing values in cannula signal leading to obstruction

(b) One accidental normal breath in a row of obstructed breaths

(c) One accidental obstructed breath in a row of normal breaths

Figure 5.9: Exceptions

5.2.3 Predictions

When the best lower and upper thresholds were found (as described in Section 5.2.1), lines 11-37 of Algorithm 7 are used for the validation set as well. For each feature prediction for each sample is being stored. Then the median of predictions (between all features) for each sample is being taken to be the final prediction.

5.2.3.1 Defining cyclic periods

In order to measure the performance of different models in classifying only the cyclic periods, there has to be a way of defining those periods using the cannula signal. Algorithm 8 was used to find them.

Algorithm 8 Finding cyclic periods

```
min ← The minimum number of breaths of one class is set to 3
max ← The maximum number of breaths of one class is set to 4
all_breaths ← The cannula signal of all breaths
for breath in all_breaths do
    if breath is normal and has at least min obstructed breaths before it
            and at least min − 1 normal breaths after it then
        if breath has a range ratio of 1.5 with the previous min breaths then
            cyclic period found
            set the maximum number of one class breaths to be max
        end if
    end if
end for
```

This algorithm is looking for periods of obstructed breathing followed by normal breathing where the change of classes appears with a big enough change in amplitudes of the ratios in the cannula signal. In other words, a very obstructed range of breaths with an obvious recovery period as described in the Introduction. When these periods are found, the predictions based on the accelerometer values can be measured only for the cyclic breathing obstructions.

5.2.4 Results

First of all, training and validation sets were introduced by cutting approximately four fifths for the training and the remaining one for the validation set. Remember from Table 2.1 that the whole data consists of 3249 breaths, 1409 and 1840 of those are of patient 1 and patient 16, respectively.

Note that the best features found from Section 4.4 can be seen in Table 4.2. Different combinations of those features were constructed and the resulting sets are presented in Table 5.2.

First of all, the reasoning behind these sets will be established:

- **5 features, z+y**. All best y axis features shared by both patients are taken, namely 0.1*quant_accel_y*, 0.9*quant_accel_y_exp* and *mean_accel_y*. As described in Section 4.2 y axis presents unique movement to different patients, so the result might be better for taking the patients individually but not together. Two more features 0.25*quant_accel_z_ins* and *median_accel_z_ins* were added since they are shared by each patient individually and both patients data as well while showing the best results of z features in Table 4.1.

- **7 features, x+y**. Again all three y axis features as in the previous set were taken because they present great results for each patient individually (look at Table 4.1). Now more axis z features are taken adding 0.1*quant_accel_z_ins* and 0.75*quant_accel_z_ins* in order to give more weight to z axis in contrast to the previous set.
- **9 features, z+x**. Here none of the y axis features are taken in order to check whether that affects the total and individual accuracies. Instead of that, some x axis features were taken, namely 0.1*quant_accel_x_ins* and *mean_accel_x_ins*. Note that from Table 4.1 it can be seen that these two features do not show the best results for patient 1 individually but yield 86.69% and 87.50% for both patients, respectively. Also, they are representative for patient 16 presenting accuracies over 90%. Features including z axis include the ones from the previous set and adding 0.9*quant_accel_z_ins* and *min_accel_z_ins* to give even more weight on the most representative axis.
- **5 features, z**. This set consists only of the features that are shared between both patients and each patient individually. These are the first five in Table 4.2.
- **3 features, y**. The set consists only the y axis features found to be the best for each patient individually in Table 4.2. As mentioned, this axis presents unique results for each patient individually, so the effect of only predicting with respect to three features 0.1*quant_accel_y*, 0.9*quant_accel_y_exp* and *mean_accel_y* is wanted to be examined.
- **13 features, x+y+z**. Now all axes are taken into account. Now features yielding the best results for both patients together are taken. These are the last column of Table 4.2. In addition to this, the 3 best y axis features are included, namely 0.1*quant_accel_y*, 0.9*quant_accel_y_exp* and *mean_accel_y*. The purpose of this set is to check whether taking features extracted from all axes show better results that disregrading one of them.
- **15 features, x+y+z**. All features from Table 4.2 were taken.

All these sets were taken separately and 5-fold cross validation was used to measure the performance of the Ratios algorithm. Only folds containing more than 20 breaths defined as cyclic were taken to measure the 5-fold cyclic accuracy in order to achieve generalized results. One more thing that must be mentioned is that the lower and higher thresholds for defining the cyclic period were taken to be three and four, respectively (described in Section 5.2.3.1). The resulting accuracies can be seen in Table 5.3.

Note that the best result found for both patients was using 15 features and yielding accuracies of 92.77% and 75.12% for cyclic and all breaths, respectively. It is clear that all feature sets include accelerometer z axis which is considered to be the most representative for both patients since it corresponds to abdomen up-and-down movement.

Note that as discussed in Section 4.2 accelerometer y axis presents good results for each patient uniquely. An attempt at predicting breaths based on only three best y axis feature was made; however, it can be seen in Table 5.3 that using only this axis is not enough even for individual patients. The cyclic accuracies for patient 1 and patient 16 were 87.47% and 93.10%, respectively which is much worse for patient 1 and relatively worse for patient 16 comparing with the performance of other sets. On

the other hand, it can be noticed from Table 5.3 that the accuracy of cyclic breaths of patient 16 is improved from 91.64% to 94.46% when axis y is added (taking sets **9 features, z+x** and **7 features, z+y**). Meanwhile, comparing the same two sets with respect to both patients the accuracy drops from 91.32% to 91.19% which is not big of a change. This also suggests that for patient 16 y axis is quite important showing that for all sets which include y axis features, the cyclic accuracies improve. Note that it is not the case for all breaths. Feature sets including 5 and 9 features with no y axis yield 73.82% and 73.38%, respectively while sets with y axis, namely **7 features, z+y** and **5 features, z+y** produce lower by 1% results. This analysis proves the hypothesis that y axis features might improve the individual accuracy of a patient but when all patients are considered, the total accuracy drops insignificantly.

Another interesting observation is that x axis improves the accuracies for cyclic and all breaths for both patients. However, if patients are considered separately, it can be noticed that for patient 16, the cyclic accuracy drops. On the other hand, the overall accuracy for all breaths of patient 16 increases when x axis features are added from 72.02% to 73.38% when considering sets **5 features, z+y** and **9 features, z+x**, respectively. For patient 1 both cyclic and all breaths accuracies improve when adding x axis features which concludes that x axis can be used in order to get better results for both patients together and sometimes for each person individually.

By this discussion it can be concluded that each axis is representative and their features can be used for predicting obstructions of breaths. Other two sets of features including different combinations of x, y and z axes were formed as it can be seen in Table 5.2. The best feature set is found to be: 0.1*quant_accel_z_ins*, 0.25*quant_accel_z_ins*, 0.75*quant_accel_z_ins*, *mean_accel*$_z$*_ins*, *median_accel_z_ins*, 0.1*quant_accel_y*, 0.9*quant_accel_y_exp*, *mean_accel_y*, *min_accel_y*, *min_accel_z_ins*, 0.25*quant_accel_y*, 0.75*quant_accel_y*, 0.25*quant_accel_x_ins*, *mean_accel_x_ins*, *median_accel_x_ins* with all and cyclic breaths accuracies being 75.12% and 92.77%, respectively. This proves that all features found in Table 4.2 are representative and should be used when finding cyclic patterns of breathing.

5.2.5 Problems and improvements

- This model has some issues regarding the connectivity between classes of breaths. One of those would be that if some breaths are not of representative pattern and get classified incorrectly, breaths following that one might be misclassified as well. This happens because of the fact that the class is being inherited from previous prediction if no significant changes in features appear (following Algorithm 7). If there exist long periods of the same class and some breaths are being incorrectly classified in the beginning, this might lead to the whole sequence of one class breaths being misclassified.
- Since predictions depend on previous breaths, breathing periods must be continuous. Data used in this project deprives this property which leads to a reasoning that the model would work even better in real-life setting where breaths are not interrupted and the predictions are being made continuously.

Feature	5 feat, z+y	7 feat, z+y	9 feat, z+x	5 feat, z	3 feat, y	13 feat, x+y+z	15 feat, x+y+z
$0.1quant\_accel\_x\_ins$			✓				
$0.1quant\_accel\_y$	✓	✓			✓	✓	✓
$0.1quant\_accel\_z\_ins$		✓	✓	✓		✓	✓
$0.25quant\_accel\_x\_ins$			✓			✓	✓
$0.25quant\_accel\_y$							✓
$0.25quant\_accel\_z\_ins$	✓	✓	✓	✓		✓	✓
$0.75quant\_accel\_y$							✓
$0.75quant\_accel\_z\_ins$		✓	✓	✓		✓	✓
$0.9quant\_accel\_y\_exp$	✓	✓			✓	✓	✓
$0.9quant\_accel\_z\_ins$			✓				
max_accel_y							
$mean\_accel\_y$	✓	✓			✓	✓	✓
$mean\_accel\_x\_ins$			✓			✓	✓
$mean\_accel\_z\_ins$				✓		✓	✓
$median\_accel\_x\_ins$						✓	✓
$median\_accel\_y$							
$median\_accel\_z\_ins$	✓	✓	✓	✓		✓	✓
$min-mean\_accel\_z$							
$min\_accel\_x\_ins$							
min_accel_y						✓	✓
$min\_accel\_z\_ins$			✓			✓	✓
$std\_accel\_x\_ins$							

Table 5.2: Feature sets (note that feat corresponds to features)

Features	Patient 1 all	Patient 1 cyclic	Patient 16 all	Patient 16 cyclic	Both	Both cyclic
5 features, z+y	75.6%	90.62%	72.02%	96.09%	67.78%	90.38%
7 features, z+y	76.53%	90.97%	72.56%	94.46%	73.20%	91.19%
9 features, z+x	76.25%	91.00%	73.38%	91.64%	75.67%	91.32%
5 features, z	75.8%	91.80%	73.82%	91.78%	75.15%	90.35%
3 features, y	74.40%	87.47%	68.37%	93.10%	63.06	86.98%
13 features, x+y+z	76.60%	91.51%	73.60%	93.72%	75.55%	92.10%
15 features, x+y+z	76.67%	90.67%	72.84%	94.19%	75.12%	92.77%

Table 5.3: Validation accuracies of breaths

- First breath classification is being done by taking the most frequent class. 5-fold cross-validation used in this project had to determine the first breath five times which might have led to more misclassifications because of the first problem defined in this section. Again, this is not a problem in a continuous measuring settings and live predictions could be more accurate.
- Undoubtedly, even if there was a big number of breaths considered, the variety of patients would still be important in order to have more robust results. Two patients data was not enough and it would be advised to conduct another study with more patients showing cyclic breathing obstruction periods. Some of the folds of patient 1 that were used to validate the method consisted of a very small number of cyclic obstruction periods since only 17.67% of this patient's data was cyclic obstruction periods. This leads to a lack of robustness with respect to each misclassified breath. Again, more data with cyclic obstructions would make the model more robust and generalizable.

Chapter 6

Conclusion

Two different models, namely Shapelets and Ratios methods, where carefully analyzed and implemented for detecting obstructed and normal breaths. Note that the Shapelets method described in Section 5.1 turned out to be not the best way to go when measuring the differences between two classes. The reason behind this is the inconsistent variance between the shapes of the accelerometer values which consequently lead to the breathing signal being variable as well. As described in Section 4.1, these different occurrences of shape patterns (curve going up and down) are caused by the body shapes of each person and are not showing distinguishable patterns when the obstruction in nasal cannula signal appears. Nevertheless, the method achieved the highest accuracy of 77.08% using the z axis of accelerometer. Another idea was taken into account which is called the Ratios method and is based on finding noticeable changes in the scaling of signals while tuning the best thresholds using machine learning (description in Section 5.2). The main difference between this method compared with the Shapelets one is the continuity of the data. When considering the Shapelets method all predictions were made independently with respect to other breaths whereas the Ratios method takes previous breaths into account when predicting the class. For this reason, the notion of cyclic obstruction periods was taken into consideration and the cyclic accuracy (defining cyclic periods is presented in Algorithm 8) was measured in parallel to all breaths accuracy. The best found algorithm presented the accuracies of 75.12% and 92.77% for all and cyclic breaths, respectively. The feature set used consisted of $0.1quant\_accel\_z\_ins$, $0.25quant\_accel\_z\_ins$, $0.75quant\_accel\_z\_ins$, $mean\_accel_z\_ins$, $median\_accel\_z\_ins$, $0.1quant\_accel\_y$, $0.9quant\_accel\_y\_exp$, $mean\_accel\_y$, min_accel_y, $min\_accel\_z\_ins$, $0.25quant\_accel\_y$, $0.75quant\_accel\_y$, $0.25quant\_accel\_x\_ins$, $mean\_accel\_x\_ins$, $median\_accel\_x\_ins$ and the accuracies reported are the ones of using 5-fold cross-validation.

In conclusion, an automatic model detecting obstructed and normal breathing with a focus on cyclic obstructions was found and could be used when monitoring breathing continuously. Since the obstructions considered in this project have similar patterns as in sleep apnea breathing, implementing this automatic detection as a real-time measurement could lead to obstructed breathing in such patients being detected automatically. Similarly, measures for preventing patients from post-operative hospital deaths

[34] could be taken in advance. Undoubtedly, there is always some room for pushing even the best models to perform more accurately. Some suggestions of how this project could be further improved are included in the next section.

6.1 Future work

Possible approaches on improving the accuracy could be made and described in this Section.

6.1.1 Grouping shapes

One idea on how to face the problems arising from the Shapelets method would be grouping and analyzing all accelerometer inspirations shapes based on the nasal cannula shapes described by T.Aittokallio et al. [29] and visualized in Figure 3.1. However, for this analysis, all marks defining the start and end of inspirations must be very precise which sometimes was not the case in the One-speck study. By doing this with more research done in the body shapes (described in Section 4.2) effect on the accelerometer values, some insights in either the shape or the gradient of an increase or decrease could be established as it was tried to do using the Pearson's correlation coefficient.

6.1.2 Weighted Ratios method

The Ratios method has never been used before this project which leads to a reasoning that there can be improvements made into building even a better version of this new algorithm. One future improvement that could be done to achieve even greater results of the Ratios model is using weights. In other words, each preceding breath could be given a weight of how important it is in a breath prediction. For example, for a particular breath later preceding breaths are more important than the older ones which means there should me more weight given to the later breaths, and vice versa. A further improvement could be made to use a probabilistic version of this which would set the weights to be based on preceding breaths which would change the deterministic Ratios model to a dynamic one.

6.1.3 Alert system

The aim of this project was to find an accurate detection of obstructed breaths using continuous data with a possible real-time implementation in the future. However, to detect the seriousness of the obstructions found, some measure causing the system to make an alert must be thought of. Analysis on a similar informing system using two devices of which one is nasal cannula was made [35] but the number of false alarms was too high for it to be a reliable measure of seriousness of the problem. With a help

of experts who are able to define the severity of the breathing obstructions an alert system could be invented using the RESpeck monitor which would produce an alert if this seriousness measure is crossed and actions could be considered in order to face the problem in advance.

Bibliography

[1] L. C. Looi-Lyons, F. F. Chung, V. W. S. Chan, and M. McQuestion, "Respiratory depression: an adverse outcome during patient controlled analgesia therapy.," *Journal of clinical anesthesia*, vol. 8 2, pp. 151–6, 1996.

[2] M. H. J. Roozekrans, R. van der Schrier, L. P. H. J. Aarts, E. Y. Sarton, M. van Velzen, M. Niesters, A. Dahan, and E. Olofsen, "Benefit versus severe side effects of opioid analgesia: Novel utility functions of probability of analgesia and respiratory depression.," *Anesthesiology*, vol. 128 5, p. 2, 2018.

[3] R. W. Byard and J. D. Gilbert, "Narcotic administration and stenosing lesions of the upper airway–a potentially lethal combination.," *Journal of clinical forensic medicine*, vol. 12 1, pp. 29–31, 2005.

[4] D. Catley, C. Thornton, C. R. Jordan, J. Lehane, D. A. Royston, and J. G. Jones, "Pronounced, episodic oxygen desaturation in the postoperative period: its association with ventilatory pattern and analgesic regimen.," *Anesthesiology*, vol. 63 1, p. 1, 1985.

[5] B. Walder, M. Schafer, I. Henzi, and M. R. Tramèr, "Efficacy and safety of patient-controlled opioid analgesia for acute postoperative pain. a quantitative systematic review.," *Acta anaesthesiologica Scandinavica*, vol. 45 7, pp. 795–804, 2001.

[6] L. A. Lynn and J. P. Curry, "Patterns of unexpected in-hospital deaths: a root cause analysis," in *Patient safety in surgery*, p. 14, 2011.

[7] Y. Gasche, Y. Daali, M. Fathi, A. Chiappe, S. R. Cottini, P. V. C. Dayer, and J. A. Desmeules, "Codeine intoxication associated with ultrarapid cyp2d6 metabolism.," *The New England journal of medicine*, vol. 351 27, pp. 2827–31, 2004.

[8] H. S. Smith, "Opioid metabolism.," *Mayo Clinic proceedings*, vol. 84 7, pp. 613–24, 2009.

[9] A. Dahan, E. Y. Sarton, L. J. Teppema, and C. N. Olievier, "Sex-related differences in the influence of morphine on ventilatory control in humans.," *Anesthesiology*, vol. 88 4, pp. 903–13, 1998.

[10] Y. Caraco, J. L. Sheller, and A. J. J. Wood, "Impact of ethnic origin and quinidine coadministration on codeine's disposition and pharmacodynamic effects.," *The*

Journal of pharmacology and experimental therapeutics, vol. 290 1, pp. 413–22, 1999.

[11] I. A. Ayappa, R. G. Norman, M. Suryadevara, and D. M. Rapoport, "Comparison of limited monitoring using a nasal-cannula flow signal to full polysomnography in sleep-disordered breathing.," *Sleep*, vol. 27 6, pp. 1171–1179, 2004.

[12] S. J. Heitman, R. S. Atkar, E. A. Hajduk, R. A. Wanner, and W. W. Flemons, "Validation of nasal pressure for the identification of apneas/hypopneas during sleep.," *American journal of respiratory and critical care medicine*, vol. 166 3, pp. 386–91, 2002.

[13] R. G. Norman, M. M. Ahmed, J. A. Walsleben, and D. M. Rapoport, "Detection of respiratory events during npsg: nasal cannula/pressure sensor versus thermistor.," *Sleep*, vol. 20 12, pp. 1175–1184, 1997.

[14] T. Aittokallio, O. Nevalainen, U. Pursiheimo, T. Saaresranta, and O. Polo, "Classification of nasal inspiratory flow shapes by attributed finite automata," *Computers and biomedical research, an international journal*, vol. 32 1, pp. 34–55, 1999.

[15] G. Drummond, A. M. Bates, J. F. E. Mann, and D. K. Arvind, "Characterization of breathing patterns during patient-controlled opioid analgesia.," *British journal of anaesthesia*, vol. 111 6, pp. 971–978, 2013.

[16] J. Hayano, E. Watanabe, Y. Saito, F. Sasaki, K. Fujimoto, T. Nomiyama, K. Kawai, I. Kodama, and H. Sakakibara, "Screening for obstructive sleep apnea by cyclic variation of heart rate.," *Circulation. Arrhythmia and electrophysiology*, vol. 4 1, pp. 64–72, 2011.

[17] H. D. Trang, V. Leske, and C. Gaultier, "Use of nasal cannula for detecting sleep apneas and hypopneas in infants and children.," *American journal of respiratory and critical care medicine*, vol. 166 4, 2002.

[18] P. D. A. Lorna Bernard, "Innovative, real-time respiratory monitoring community clinical study," 2012.

[19] C. E. D. Limited, "Spike 2 life sciences data acquisition analysis system." http://ced.co.uk/products/spkovin. [Online; accessed 2019/04/02].

[20] A. Bates, D. K. Arvind, and J. Mann, "Wireless monitoring of post-operative respiratory complications," in *Wireless Health*, 2011.

[21] Z. B. H. Siti Farah Binti Hussin, Gauri a/p Birasamy, "Design of butterworth band-pass filter.," *Engineering and Technology*, vol. 1, p. 13, 2016.

[22] P. de Chazal, T. Penzel, and C. Heneghan, "Automated detection of obstructive sleep apnoea at different time scales using the electrocardiogram.," *Physiological measurement*, vol. 25 4, pp. 967–983, 2004.

[23] "Polysomnography in patients with obstructive sleep apnea: an evidence-based analysis.," *Ontario health technology assessment series*, vol. 6 13, p. 9, 2006.

[24] T. Kim, J.-W. Kim, and K. Lee, "Detection of sleep disordered breathing severity using acoustic biomarker and machine learning techniques," in *Biomedical engineering online*, 2018.

[25] A. Gotter, "Pulse oximetry." https://www.healthline.com/health/pulse-oximetry, 2017. [Online; accessed 2018/12/28].

[26] L. Almazaydeh, M. Faezipour, and K. Elleithy, "A neural network system for detection of obstructive sleep apnea through spo2 signal features," 2012.

[27] L. Almazaydeh, K. M. Elleithy, and M. Faezipour, "Obstructive sleep apnea detection using svm-based classification of ecg signal features," *2012 Annual International Conference of the IEEE Engineering in Medicine and Biology Society*, pp. 4938–4941, 2012.

[28] D. S. T. T. J. V. Leah Baron, Thomas Decker, "Foundation safety innovations: Virtua health: Implementing capnography in low acuity settings." http://bernoullihealth.com/wp-content/uploads/2016/03/2016_SI_Virtua_Capnography.pdf, 2016. [Online; accessed 2018/12/28].

[29] T. Aittokallio, T. Saaresranta, P. Polo-Kantola, O. P. O. Nevalainen, and O. Polo, "Analysis of inspiratory flow shapes in patients with partial upper-airway obstruction during sleep.," *Chest*, vol. 119 1, pp. 37–44, 2001.

[30] L. Ye and E. J. Keogh, "Time series shapelets: a new primitive for data mining," in *KDD*, 2009.

[31] L. R. R. K. R. Delaram Yazdansepas, Nitin Saroha, "Towards efficient real-time human activity recognition using wearable sensors: A shapelet-based pattern matching approach," in *BODYNETS '18*, 2018.

[32] J. Murphy, "Detecting obstructed breathing episodes with respiratory data from post-operative patients," master thesis, The University of Edinburgh, 2018.

[33] E. J. Keogh, L. Wei, X. Xi, S.-H. Lee, and M. Vlachos, "Lb_keogh supports exact indexing of shapes under rotation invariance with arbitrary representations and distance measures," in *VLDB*, pp. 882–893, 2006.

[34] J. Silber, S. V. Williams, H. Krakauer, and J. S. Schwartz, "Hospital and patient characteristics associated with death after surgery. a study of adverse occurrence and failure to rescue.," *Medical care*, vol. 30 7, pp. 615–629, 1992.

[35] L. M. Wiklund, B. Hök, K. Stahl, and A. Jordeby-Jönsson, "Postanesthesia monitoring revisited: frequency of true and false alarms from different monitoring devices.," *Journal of clinical anesthesia*, vol. 6 3, pp. 182–8, 1994.